

| Topic | Moment tensor inversion and moment tensor interpretation |
|---------|---|
| Authors | Torsten Dahm , Helmholtz Centre Potsdam GFZ German Research Centre for Geosciences and University of Potsdam, Institute of Earth and Environmental Sciences, Germany; E-mail: torsten.dahm@gfz-potsdam.de Frank Krüger , University of Potsdam, Institute of Earth and Environmental Sciences, 14476 Potsdam, Germany; E-mail: Frank.Krueger@geo.uni-potsdam.de |
| Version | January 2014; DOI: 10.2312/GFZ.NMSOP-2_IS_3.9 |

| | page |
|--|------|
| 1 Introduction | 1 |
| 1.1 Nomenclature and terms | 2 |
| 2 Moment tensors: Interpretation and decomposition | 3 |
| 2.1 Elementary physical sources | 5 |
| 2.1.1 The isotropic source (explosion and implosion) | 5 |
| 2.1.2 The general dislocation source | 5 |
| 2.1.3 The shear dislocation source | 6 |
| 2.1.4 The tensile crack | 7 |
| 2.2 Decomposition into elementary sources | 7 |
| 2.2.1 Decomposition into strike slip, dip slip DC sources and a vertical CLVD | 8 |
| 2.2.2 Decomposition into a best double couple and a CLVD | 9 |
| 2.2.3 Decomposition into an isotropic source and a mixed-mode shear-tensile crack | 10 |
| 2.3 Computer programs for decomposition | 10 |
| 2.4 Displaying different moment tensor components | 12 |
| 3 Moment tensor representations: basic relations | 13 |
| 3.1 Resolving the time dependency of moment tensors | 16 |
| 3.2 Representation of the centroid location (centroid moment tensor inversion) | 18 |
| 3.3 Representation in a layered Earth model | 20 |
| 3.4 Representation for body waves (peak amplitudes and amplitude ratios) | 22 |
| 3.5 Relative moment tensor inversion using multiple events (body wave method) | 24 |
| 3.6 Full waveform method using amplitude spectra | 24 |
| 3.7 Moment tensor representation using eigen-vibrations and eigen-modes of the Earth | 25 |
| 3.8 Codes to calculate Green functions for moment tensor inversion | 26 |
| 4 Moment tensor inversions: schemes in practice | 27 |
| 5 Free packages for moment tensor inversion | 28 |
| 6 Moment tensor catalogues | 30 |
| 7 Acknowledgments | 33 |
| 8 References | 33 |

1 Introduction

The following brief guide to moment tensor inversion discusses the characteristics of moment tensors, its physical interpretation and the different ways to decompose moment tensors. It reviews the basic equations used in different inversion schemes, clarifies the role of Green's

functions, and summarizes different practical aspects of moment tensor inversions for different types of waves and different distance ranges (local, regional and global earthquakes). Typical resolution problems of moment tensor components are discussed. The IS provides some guidelines to start moment tensor studies, and thereby introduces a modern, python based moment tensor toolbox (Kiwi Tools) that is flexible to adapt to all specific source studies and incorporates pre-calculated Green's function databases. The complementing exercise EX 3.6 provides a practical on moment tensor inversion using the Kiwi Tools. The IS does not derive the fundamental concepts and the theory of source representations, since this is given in chapter 3 and IS3.1 of the NMSOP-2.

The material is based in large parts on a review paper by Jost and Herrmann (1989) and on lecture notes and practicals we developed during several training courses on moment tensors between 2000 and 2012 (e.g. ESC and IUGG training courses, ICTP workshops in Trieste, Winterschool Sudelfeld). The material updates and extends IS3.8 in NMSOP by Günther Bock on moment tensor determination and decomposition.

1.1 Nomenclature and terms

The following nomenclature is used (unit in parentheses):

Table 1: Nomenclature

| Parameter | Explanation | Type |
|---|--|---|
| t and τ | Time, referenced to receiver and source, respectively | Scalars (s) |
| ω | Angular frequency | Scalar (rad) |
| \mathbf{x} and ξ | Spatial coordinates of source and receivers | Vectors (m) |
| \mathbf{M} and \mathbf{m} | Moment tensor and moment tensor density | 2 nd rank tensors, (Nm and Nm/m ²) |
| \mathbf{G} | Green's tensor | 3 rd rank tensor (m) |
| \mathbf{u} and \mathbf{D} | Displacement and dislocation across fault | Vectors (m) |
| \mathbf{c} | Elasticity tensor | 4 th rank tensor (Pa) |
| A and V | Surface and volume of source | Scalars (m ² and m ³) |
| $\phi, \varphi, \lambda, \delta, \alpha, \beta$ | Angles | Scalars (rad) |
| δ, δ or δ_{ij} | Kronecker symbol, see e.g. IS3.1 | Scalar or 2 nd rank tensor |
| N, η, K | 1 st and 2 nd Lame's constant and bulk modul | Scalars (Pa) |
| \mathbf{F} and \mathbf{f} | Point force and force density | Vector (N or N/m ³) |
| r | Distance | Scalar (m) |
| γ | Direction cosine | Vector (rad) |
| \mathbf{n}, \mathbf{l} | Unit vectors (e.g. fault normal or slip direction) | |
| \mathbf{s} | Slowness vector | Vector (s/m) |
| \mathbf{e} | Eigenvalue vector of moment tensor | Vector (Nm) |
| h(t) | Source time function of the point source | Dimensionless |

We use bold face letters (e.g. \mathbf{x}) to express vectors and tensors. Scalars are denoted in normal (not bold face) letters. Components of vectors and tensors are denoted by x_i and M_{ij} , respectively, where indices usually vary between 1, 2, and 3. We further apply the Einstein summation convention, meaning that repeating indices in one term imply summation over the index, i.e. $e_k n_k = \sum e_i n_i = e_1 n_1 + e_2 n_2 + e_3 n_3$. Indices separated by comma "," denote partial

derivatives to space coordinates, i.e. $G_{ij,k} = \partial G_{ij}/\partial x_k$. Note that the summation convention will also apply to terms like M_{kk} or $M_{kj} G_{ik,j}$. The * symbol denotes a **temporal convolution integral** and we partly drop the implicit time variable in the convolution formulas, e.g.,

$$\int_{\tau=-\infty}^t M(\xi, \tau)G(x, \xi, t - \tau)d\tau = M(\xi, t) * G(x, \xi, t) = M(\xi) * G(x, \xi)$$

2 Moment tensors: interpretation and decomposition

Moment tensors provide a general theoretical framework to describe seismic sources based on generalized force couples (Fig. 1). The moment tensor description is not restricted to earthquake sources, but covers also other types of seismic sources such as explosions, implosions, rock falls, landslides, meteorite terminal explosions (e.g. atmospheric), and mixed mode ruptures driven by fluid and gas injections. Thus, the concept of moment tensors is quite general and flexible making moment tensor inversions a very important tool in seismic source characterization. Moment tensors have the potential to substitute other, more traditional, source parameter estimations, such as e.g. magnitude or focal solutions from first motion polarities.

We denote a point source moment tensor by \mathbf{M} , a moment tensor density by \mathbf{m} . A moment tensor \mathbf{M} defines the strength of a seismic source in terms of its seismic moment, usually denoted by the scalar quantity M_0 , and the radiation pattern of seismic waves. The moment tensor (3x3 matrix) is symmetric, i.e. it has six independent components. The diagonal elements represent linear vector dipoles, the off diagonal elements represent the force couples with arms (moment) (Fig. 1).

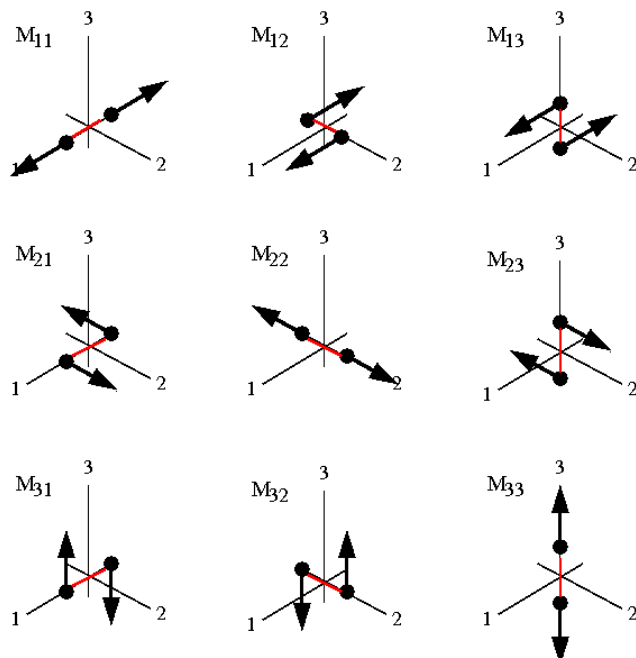


Figure 1 The system of force couples representing the components of a Cartesian moment tensor. Diagonal elements of the moment tensor represent linear vector dipoles, while off-diagonal elements represent force couples with moment.

The moment tensor has components M_{ij} where $i,j = 1,2$, or 3. Often, a local geographic coordinate system is used to define a Cartesian system tensor, with positive x_1 being north-, positive x_2 eastward, and positive x_3 being downward (NED). The NED coordinate system is used below to derive relations between the angles of a ruptured fault (strike and dip angle) and the dislocation direction on the rupture plane (rake angle).

A system commonly used in free-oscillation analysis is a local $r\text{-}\Theta\text{-}\Phi$ -system, with r , Θ , Φ pointing upward, southward, and eastward (USE), respectively. This system is used for the routinely reported Global Centroid Moment tensors (Global CMT, formerly Harvard CMT). The geographic Cartesian tensor (NED) transforms by:

$$\begin{aligned} M_{rr} &= +M_{zz}, & M_{\Theta\Theta} &= +M_{nn}, & M_{\Phi\Phi} &= +M_{ee}, \\ M_{r\Theta} &= +M_{nz}, & M_{r\Phi} &= -M_{ez}, & M_{\Theta\Phi} &= -M_{ne}. \end{aligned} \quad (1)$$

Additional coordinate systems in use are ENU (e.g. Jost and Herrmann, 1989) and NWU (e.g. Box 8.3 in Lay and Wallace, 1995 and section 4.2.1 in Stein and Wysession, 2003). Different definitions lead to a different ordering and polarities of individual matrix components of the tensor. A wrong association may lead to mis-interpretation of components and fault directions. Therefore, the coordinate system should always be published together with the moment tensor solution.

With the exception of microseisms (ambient noise), earthquakes or explosions are the most common localized sources for seismic waves in the Earth. Other source such as tensile cracks, rock bursts or mass slope are significant sources close to the Earth's surface or in regions under high fluid overpressure (e.g. at volcanoes). All internal sources can be represented by a specific combination of generalized force couples (moment tensor components), which radiate at low frequencies the same waves as, for instance, the dislocation process on the geological fault. Having estimated a moment tensor, a decomposition and interpretation of the moment tensor is often needed to find the most appropriate geological or physical source process. In general, two concepts are followed when decomposing moment tensors:

- (1) the decomposition into physical (geological) source components to aid interpretation, for instance explosions, shear and tensile cracks or
- (2) the purely mathematical decomposition as a technique to simplify the inversion or numerical analysis.

We briefly introduce the source representations of the most elementary physical sources and then discuss different decompositions.

2.1 Elementary physical sources

2.1.1 The isotropic source (explosion and implosion)

$$\mathbf{M}_{iso} = \Delta V (\eta + 2N) \begin{pmatrix} 1 & 0 & 0 \\ 0 & 1 & 0 \\ 0 & 0 & 1 \end{pmatrix}.$$

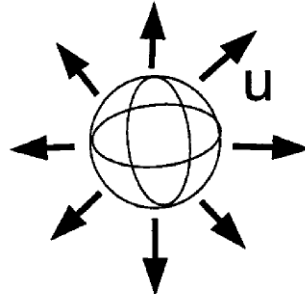


Figure 2 Shape and radiation of the isotropic (volumetric) moment tensor

An explosion in a drill hole at depth is associated with abrupt volume change. In terms of pressure and force dipoles it is represented by an abrupt, isotropic pressure change and by means of three orthogonal linear force dipoles, respectively (see Fig. 2). The explosion (or implosion) radiates, theoretically, P waves with equal amplitude and polarity in all directions (isotropic source). S waves are not excited by the buried isotropic source. Most often, the polarity of the P wave radiation is plotted to visualize the radiation of the source. The lower hemisphere of a virtual sphere around the source is projected in a horizontal plane; examples and explanations are given in, e.g., chapter 3 of the NMSOP-2. The radiation pattern plot of an isotropic source is then a uni-colored sphere (black for explosion and white for implosion).

The only free parameter of the isotropic moment tensor, \mathbf{M}_{iso} , is the pre-factor of the unity matrix in Fig. 2, which defines the strength, or moment $M_0 = tr = (M_{11}+M_{22}+M_{33})/3$, of the isotropic source. Knowing M_0 and the elastic constants N and η (see table 1) of the rocks at the source, the volume change ΔV of the explosion or implosion source can be estimated by

$$tr = (M_{11}+M_{22}+M_{33}) / 3 = \Delta V (\eta + 2N) \quad (\text{explosion}) \quad (2)$$

Note that dislocation sources can also generate isotropic components in the radiation pattern of the source. The volume change associated with these sources is, however, different to equation (2) (see Müller, 1973, 2001) and given below. Note further that the moment of an explosion in the atmosphere has to be treated differently (e.g., Heimann et al., 2013).

2.1.2 The general dislocation source

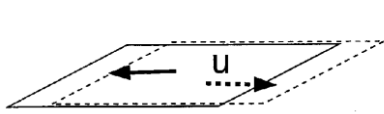


Figure 3a: Dislocation of a shear crack with $\mathbf{n}=(0,0,1)$ and $\mathbf{D}_S=(0,-1,0)$.

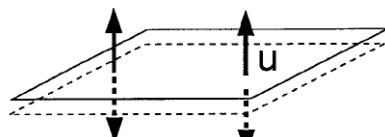


Figure 3b: Dislocation of a tensile crack with $\mathbf{n}=(0,0,1)$ and $\mathbf{D}_N=(0,0,1)$.

A source associated with a planar crack and a dislocation vector \mathbf{D} in an arbitrary direction (shear as well as opening mode, see Fig. 3) may be termed a "general dislocation source". While tectonic earthquakes rupture in pure shear mode, rupture under the presence of fluids with high overpressure may involve an additional opening of the rupture plane. This may occur during magma- or fluid-intrusions, although the validity of observations of mixed-mode rupture are often debated among experts. The moment tensor of a general dislocation source is (eq. 3.21 in Aki and Richards, 2002)

$$M_{pq} = N A (n_p D_q + n_q D_p) + \eta A n_k D_k \delta_{pq} \quad (3)$$

The general dislocation source has five independent parameters. Equation (3) can be described in terms of strike (ϕ), dip (δ), rake (λ), and the magnitudes of the shear (D_S) and opening (D_N) dislocation. If the moment tensor is defined in a NED system the relation to these parameters is (e.g., Dahm, 1998)

$$\begin{aligned} M_{11}/A &= -D_S N (\sin 2\phi \sin \delta \cos \lambda + \sin^2 \phi \sin 2\delta \sin \lambda) & +D_N (\eta + 2N \sin^2 \phi \sin^2 \delta) \\ M_{12}/A &= +D_S N (\cos 2\phi \sin \delta \cos \lambda + 0.5 \sin 2\phi \sin 2\delta \sin \lambda) & -D_N N \sin 2\phi \sin^2 \delta \\ M_{13}/A &= -D_S N (\cos \phi \cos \delta \cos \lambda + \sin \phi \cos 2\delta \sin \lambda) & +D_N N \sin \phi \sin 2\delta \\ M_{22}/A &= +D_S N (\sin 2\phi \sin \delta \cos \lambda - \cos^2 \phi \sin 2\delta \sin \lambda) & +D_N (\eta + 2N \cos^2 \phi \sin^2 \delta) \\ M_{23}/A &= -D_S N (\sin \phi \cos \delta \cos \lambda - \cos \phi \cos 2\delta \sin \lambda) & -D_N N \cos \phi \sin 2\delta \\ M_{33}/A &= +D_S N \sin 2\delta \sin \lambda & +D_N (\eta + 2N \cos^2 \delta) \end{aligned} \quad (4)$$

2.1.3 The shear dislocation source

The shear dislocation source is a special case of (4) if $D_N=0$ and is usually associated with a tectonic earthquake. It has four independent parameters. The earthquake rupture is an expression of the rapid dislocation (described by the rake angle and slip) of the two surfaces of a geological fault (described by strike and dip angles) relative to each other. The rupture plane of an earthquake may become quite large if the earthquake is strong. For instance, a magnitude M_w 6 earthquake may rupture a fault of several kilometer length. The ruptured portion of the geological fault is usually approximated by a plane of area A , e.g. with length L and width W . The earthquake source is therefore idealized by the physical model of a "planar shear crack" or "shear dislocation" source. In terms of forces, a shear crack can be represented by two perpendicular force dipoles with zero angular momentum. Therefore, the shear crack source is often termed "double couple" (DC). Fig. 3a gives an example of a shear dislocation on a horizontal plane with the associated moment tensor,

$$\mathbf{M} = AD_S N \begin{bmatrix} 0 & 0 & 0 \\ 0 & 0 & -1 \\ 0 & -1 & 0 \end{bmatrix}, \quad (5)$$

where D_S is the average shear dislocation over the plane A . The seismic moment of the shear crack depends on the product between dislocation, the area of the ruptured plane and the shear modulus (see equation 3 and, e.g., equation 43 in IS3.1)

$$M_0 = \sqrt{(0.5 M_{pq} M_{pq})} = AD_S N \quad . \quad (6)$$

2.1.4 The tensile crack

For $D_S=0$ in equation (4) we have a pure tensile crack. The tensile crack has only three independent parameters, since the direction of the dislocation vector is always perpendicular to the rupture plane (no rake angle defined). The principal axis moment tensor of the tensile crack of Fig. 3b, for instance, is given by

$$AD_N \begin{bmatrix} \eta & 0 & 0 \\ 0 & \eta & 0 \\ 0 & 0 & \eta + 2N \end{bmatrix} = (\eta + \frac{2}{3}N)AD_N \begin{bmatrix} 1 & 0 & 0 \\ 0 & 1 & 0 \\ 0 & 0 & 1 \end{bmatrix} + \frac{2}{3}AD_N N \begin{bmatrix} -1 & 0 & 0 \\ 0 & -1 & 0 \\ 0 & 0 & 2 \end{bmatrix} \quad (7)$$

The strength of the tensile crack may be defined in a similar manner as before. Calculating the volume change ΔV can be of interest, for instance to estimate the volume of the intruded material. The decomposition in equation (7) shows how the volume change is related to the isotropic component of the tensile crack, M_{iso} . Note this relation is different to equation (2) of the explosion source,

$$tr = (M_{11} + M_{22} + M_{33}) / 3 = \Delta V (\eta + 2N/3) \quad (\text{tensile crack}). \quad (8)$$

2.2 Decomposition into elementary sources

The decomposition of M_{pq} into physical sources is not unique. Several decompositions have been introduced depending on the source region and range of interpretations considered. The review paper by Jost and Herrmann (1989) gives an excellent overview and introduction to decompositions in use today. The paper describes the concepts of moment tensor decomposition, and how they can be coded by using dyadics. A brief summary is given below, and we refer to the original publication for details.

The moment tensor is first decomposed in its principal axis system

$$\mathbf{M} = \begin{pmatrix} a_{1x} & a_{2x} & a_{3x} \\ a_{1y} & a_{2y} & a_{3y} \\ a_{1z} & a_{2z} & a_{3z} \end{pmatrix} \begin{pmatrix} e_1 & 0 & 0 \\ 0 & e_2 & 0 \\ 0 & 0 & e_3 \end{pmatrix} \begin{pmatrix} a_{1x} & a_{1y} & a_{1z} \\ a_{2x} & a_{2y} & a_{2z} \\ a_{3x} & a_{3y} & a_{3z} \end{pmatrix} \quad (9)$$

Here, a_i represent eigenvectors associated to eigenvalues e_i . The next step is to split the full tensor into an isotropic and a deviatoric tensor. If \mathbf{M}' represents the moment tensor in its principal axis system with eigenvalues e_i the decomposition is

$$\begin{pmatrix} e_1 & 0 & 0 \\ 0 & e_2 & 0 \\ 0 & 0 & e_3 \end{pmatrix} = \begin{pmatrix} tr & 0 & 0 \\ 0 & tr & 0 \\ 0 & 0 & tr \end{pmatrix} + \begin{pmatrix} e_1 - tr & 0 & 0 \\ 0 & e_2 - tr & 0 \\ 0 & 0 & e_3 - tr \end{pmatrix} \quad (10)$$

with $tr = (e_1 + e_2 + e_3)/3$ being 1/3 of the trace of \mathbf{M}' and $e'_k = e_k - tr$ being the eigenvalues of the deviatoric tensor.

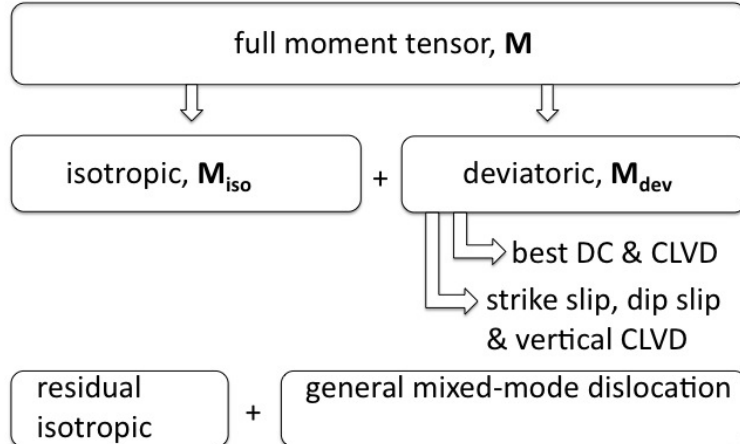


Figure 4 The two possibilities to decompose a full moment tensor, either into an isotropic and deviatoric tensor or into a general mixed-mode shear crack and a residual isotropic component. The deviatoric component can be further decomposed into different elementary sources.

The decomposition into M_{iso} and M_{dev} is unique. The M_{iso} tensor radiates only P waves, Rayleigh waves and spheroidal normal modes with no directional preference. The deviatoric tensor (M_{dev}) often has no direct geological meaning and is therefore further decomposed into different geologically reasonable sources. Several decompositions have been suggested for the deviatoric tensor, for instance (e.g. Jost and Herrmann, 1989 and Fig. 4):

- a best double-couple (DC) and a CLVD,
- a strike slip, a pure dip slip and a vertical compensated linear vector dipole (vsCLVD),
- an isotropic source and a mixed mode double couple and tensile crack on the same crack (general dislocation source).

Geologically, the first decomposition maximizing the DC part is the most relevant one in most cases.

The first step in the decomposition is the calculation of eigenvalues and eigenvectors of the seismic moment tensor. If by definition a positive isotropic tensor is associated with volume expansion, the eigenvector of the largest eigenvalue gives the direction of the T (or tensional) axis; the one of the smallest eigenvalue the direction of the P (or compressional) axis, and the eigenvector of the intermediate eigenvalue gives the direction of the null axis. The demeaned absolute values of the eigenvalues can be used to estimate the proportional strength of the different source components of the deviatoric tensor (see Jost and Herrmann, 1989).

2.2.1 Decomposition into strike slip, dip slip DC sources and a vertical CLVD

Elementary tensors that fulfil orthogonality are sometimes used instead of Cartesian components (see e.g. Aki and Richards, 2002, Box 4.4, p. 112). One possible reason is to calculate Green's functions if the available codes that cannot handle single component moment tensor excitation. Another reason might be to easily incorporate constraints during inversion.

A possible decomposition into elementary tensors are: (1) a strike-slip double-couple (\mathbf{M}_1), (2) a 90° dip-slip double-couple (\mathbf{M}_2), (3) an isotropic tensor and (4) a vertical CLVD ($\mathbf{M}_{v\text{-clvd}}$),

$$\mathbf{M} = \mathbf{M}_1(\phi_S) + \mathbf{M}_2(\phi_D) + \mathbf{M}_{iso} + \mathbf{M}_{v\text{-clvd}} \quad \text{with (in Cartesian system)}$$

$$\begin{aligned}
 \begin{pmatrix} M_{11} & M_{12} & M_{13} \\ M_{21} & M_{22} & M_{23} \\ M_{31} & M_{32} & M_{33} \end{pmatrix} &= \begin{pmatrix} -\frac{1}{2}(M_{22} - M_{11}) & M_{12} & 0 \\ M_{21} & \frac{1}{2}(M_{22} - M_{11}) & 0 \\ 0 & 0 & 0 \end{pmatrix} \\
 &+ \begin{pmatrix} 0 & 0 & M_{13} \\ 0 & 0 & M_{23} \\ M_{31} & M_{32} & 0 \end{pmatrix} \\
 &+ \frac{1}{3}(M_{11} + M_{22} + M_{33}) \begin{pmatrix} 1 & 0 & 0 \\ 0 & 1 & 0 \\ 0 & 0 & 1 \end{pmatrix} \\
 &+ \frac{1}{3}\left(\frac{1}{2}(M_{22} + M_{11}) - M_{33}\right) \begin{pmatrix} 1 & 0 & 0 \\ 0 & 1 & 0 \\ 0 & 0 & -2 \end{pmatrix}, \tag{11}
 \end{aligned}$$

The first and second term represent a strike-slip and pure dip-slip source, respectively, with strike angles ϕ_S and ϕ_D . The third term in equation (22) is the isotropic component and the forth term the vertical CLVD source. The strike slip source, \mathbf{M}_1 , has a π -periodic azimuthal radiation pattern, the dip-slip \mathbf{M}_2 a 2π -periodic, and $\mathbf{M}_{v\text{-clvd}}$ and \mathbf{M}_{iso} an azimuth-independent radiation pattern. SH-waves cannot resolve $\mathbf{M}_{v\text{-clvd}}$ and \mathbf{M}_{iso} , SV-waves are not sensitive to \mathbf{M}_{iso} , while P-waves theoretically can resolve all elementary sources. The decomposition in equation (22) can be expressed in terms of strike, dip, and rake of the best double couple, the null-eigenvalue, and the trace of the tensor (Dahm, 1993).

2.2.2 Decomposition into a best double couple and a CLVD:

The decomposition, including the isotropic component of the full tensor, is commonly expressed by

$$\begin{bmatrix} e_1 & 0 & 0 \\ 0 & e_2 & 0 \\ 0 & 0 & e_3 \end{bmatrix} = tr \begin{bmatrix} 1 & 0 & 0 \\ 0 & 1 & 0 \\ 0 & 0 & 1 \end{bmatrix} + (e_2 - tr) \begin{bmatrix} 1 & 0 & 0 \\ 0 & 1 & 0 \\ 0 & 0 & -2 \end{bmatrix} + (e_1 - e_2) \begin{bmatrix} 1 & 0 & 0 \\ 0 & 0 & 0 \\ 0 & 0 & -1 \end{bmatrix} \tag{12}$$

If e_{min} and e_{max} are the smallest and largest absolute values of e'_k (assume $|e'_3| \geq |e'_1| \geq |e'_2|$) and with $F = e_{min} / e_{max} = e'_2 / e'_3$, one may define $100(1-2F)$ as the percentage of the double couple component (between 0% and 100%, see e.g. Dziewonski et al., 1981).

The DC component (last term in 12) has been described above. A CLVD source (middle term in 12) has no verified geological representation and is for crustal earthquakes often interpreted as source component representing the residual radiation from the best double couple source. The residual radiation may result from noisy data or from simplifying assumptions, as for instance from neglecting wave effects of a 3D Earth during the inversion. Therefore, a small or zero CLVD component is sometimes interpreted as a confirmation of the model assumption.

The decomposition of the deviatoric component into best DC and CLVD is commonly used in seismology. For instance, the source mechanism reported by nearly all seismic services are based on the decomposition into a best double couple and a CLVD component. A computer program for such a decomposition is described below.

2.2.3 Decomposition into an isotropic source and a mixed-mode shear-tensile crack:

The decomposition of the principal axis tensor into M_{iso} and a general dislocation crack is

$$\begin{bmatrix} e_1 & 0 & 0 \\ 0 & e_2 & 0 \\ 0 & 0 & e_3 \end{bmatrix} = tr \begin{bmatrix} 1 & 0 & 0 \\ 0 & 1 & 0 \\ 0 & 0 & 1 \end{bmatrix} + (e_2 - tr) \begin{bmatrix} \frac{3}{2} \cos 2\phi - \frac{1}{2} & 0 & \frac{3}{2} \sin 2\phi \\ 0 & 1 & 0 \\ \frac{3}{2} \sin 2\phi & 0 & -\frac{3}{2} \cos 2\phi - \frac{1}{2} \end{bmatrix} - \frac{3}{2}(e_2 - tr) \tan 2\phi \begin{bmatrix} \sin 2\phi & 0 & \cos 2\phi \\ 0 & 0 & 0 \\ \cos 2\phi & 0 & -\sin 2\phi \end{bmatrix}, \quad (13)$$

with $\tan^2 \phi = \frac{-3(e_2 - tr) + e_3 - e_1}{3(e_2 - tr) + e_3 - e_1}$, $e_2 - tr \neq 0$.

where the angle ϕ defines the angle of the dislocation plane measured against the T axis in the plane given by the T and P axis (P and T are interchanged in case of contraction) (e.g. Dahm, 1993; Dahm and Brandsdottir, 1997). Another formulation of mixed-mode crack decomposition is given by Vavryčuk (2001).

2.3 Computer programs for decomposition

Computer programs for decomposition were written by Jost and distributed in Volume VIII of the software package “Computer Programs in Seismology” (see R. Herrmann, Saint Louis University <http://www.eas.slu.edu/People/RBHerrmann/ComputerPrograms.html>). Another computer package is provided with the python tool ”MoPaD” (Krieger and Heimann, 2012; <http://www.larskrieger.de/mopad/>), which can be used for decomposition, projection and the plotting of moment tensors. MoPaD can be easily combined with GMT plotting tools (<http://gmt.soest.hawaii.edu>).

The following examples are derived using MOPAD. On 19 March 2013 a M_L 4.2 earthquake struck the Polish mine district close to the Rudna copper mine. 19 mine workers were trapped in the mine at 850 m depth for several hours due to rock bursts affecting parts of the underground tunnels. A centroid moment tensor inversion (0.07-0.1 Hz) using broadband regional stations retrieved a seismic moment of M_W 3.8 ($M_0=5.3E14$ Nm) at a source depth of

about 1 km (Whidden et al., 2013; Rudzinski and Lizurek, pers. communication). The NED Cartesian moment tensor is decomposed into an isotropic and deviatoric part,

$$\begin{aligned}\hat{\mathbf{M}} &= 5.3 \cdot 10^{14} \text{Nm} \begin{pmatrix} -0.40 & +0.01 & -0.10 \\ +0.01 & -0.43 & +0.01 \\ -0.10 & +0.01 & -1.00 \end{pmatrix} \\ &= 5.3 \cdot 10^{14} \text{Nm} \begin{pmatrix} -0.61 & & \\ & -0.61 & \\ & & -0.61 \end{pmatrix} + 5.3 \cdot 10^{14} \text{Nm} \begin{pmatrix} +0.21 & +0.01 & -0.10 \\ +0.01 & +0.18 & +0.01 \\ -0.10 & +0.01 & -0.39 \end{pmatrix}\end{aligned}$$

The radiation pattern is plotted in a lower hemispherical projection (Fig. 5a, and chapter 3 of NMSOP-2 for explanations on the type of plots). The isotropic component is negative (implosion) and covers 60% of the moment of the full tensor.

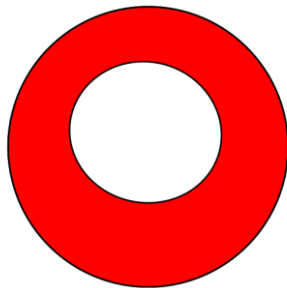


Figure 5a Lower hemispherical projection of the P-wave radiation (stereographic) of the Rudna mine 2013 Mw 3.8 moment tensor solution

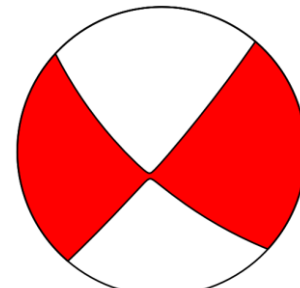


Figure 5b Lower hemispherical projection (stereographic) of the 13 Oct. 2013 Mw 6.6 Gulf of California moment tensor solution.

Apparently, the relatively slow collapse of void space in the mine building dominates the long period wave radiation and gives the major contribution of the seismic moment. The 40% deviatoric source component can be decomposed in a best double couple (DC) and a CLVD component, where the DC covers only about 13% of the size of the deviatoric tensor. The low frequency radiation pattern can therefore be interpreted in terms of an isotropic and CLVD component, where the CLVD is roughly vertically oriented. The source process may be interpreted in terms of a tensile crack as given in equation (23), by e.g.

$$AD_N \begin{pmatrix} \eta & 0 & 0 \\ 0 & \eta & 0 \\ 0 & 0 & \eta + 2N \end{pmatrix} \approx 5.3 \cdot 10^{14} \text{Nm} \begin{pmatrix} -0.4 & 0 & 0 \\ 0 & -0.4 & 0 \\ 0 & 0 & -1.00 \end{pmatrix}$$

and thus

$$AD_N = 5.3 \cdot 10^{14} \text{ Nm} \cdot 0.5(-1.0 + 0.4)/25 \cdot 10^9 \text{ N/m}^2 \approx 6360 \text{ m}^3$$

$$\eta = -0.4 \times 5.3 \cdot 10^{14} \text{ Nm}/6360 \text{ m}^3 \approx 33 \text{ GPa}$$

$$\nu = \frac{\eta}{2(\eta + N)} \approx 0.28$$

The collapsed volume AD_N can be used to estimate the area affected by the collapse if the average height of the galleries in the mine is specified. For instance, assuming the average height of the gallery is 5m, the estimated area is about 35m x 35m. The estimated Poisson ratio of 0.28 and the derived Lame's parameter may be used to check the consistency of the source interpretation with expected rock properties. Ford et al. (2008) studied a mine collapse event of a coal mine in Utah and estimated a vertical crack component of comparable relative strength.

The second example concerns the moment tensor solution of an M_w 6.6 earthquake in the Gulf of California that occurred on 13 October 2013 at a depth of 16 km. The global moment tensor solution in an USE system is (GFZ solution) is

$$\hat{\mathbf{M}} = 1 \cdot 10^{18} \text{ Nm} \begin{pmatrix} -0.59 & -2.52 & -1.72 \\ -2.52 & -7.58 & -0.95 \\ -1.72 & -0.95 & +8.16 \end{pmatrix}$$

The isotropic component is constraint to zero during inversion. The seismic moment is estimated to as 9.1E18 Nm. The DC component of the solution is 99%, meaning that the rupture can be interpreted as pure shear crack, in this case a dominant left lateral strike slip mechanism (see Fig. 5b) with strike, dip and rake of the two nodal planes of

plane 1: $\Phi = 133^\circ$, $\delta = 69^\circ$, $\lambda = -173^\circ$

plane 2: $\Phi = 40^\circ$, $\delta = 84^\circ$, $\lambda = -20^\circ$

2.4 Displaying different moment tensor components

Displaying the elementary source components in a simple graph is not trivial. Hudson et al. (1989) and Riedesel and Jordan (1998) suggested diagrams for this purpose. The Hudson et al. (1989) plot is now often used. See Tape and Tape (2012) for a geometric comparison of source-type plots. Figure 6 displays the Hudson-type plot for the two moment tensors discussed in 2.3. The pure double couple moment tensor is centered at the origin and indicates a pure DC moment tensor. The Rudna mine solution is localized in the lower half-space indicating negative isotropic source components. It is very close to a pure linear dipole solution, which further shows that the source is close to a pure collapsing crack solution. Opening cracks would appear in the positive half-space close to the positive dipole marker. Pure explosions and isotropic implosions events appear on the vertical axis of the plot frame at the points marked by +ISO and -ISO, respectively.

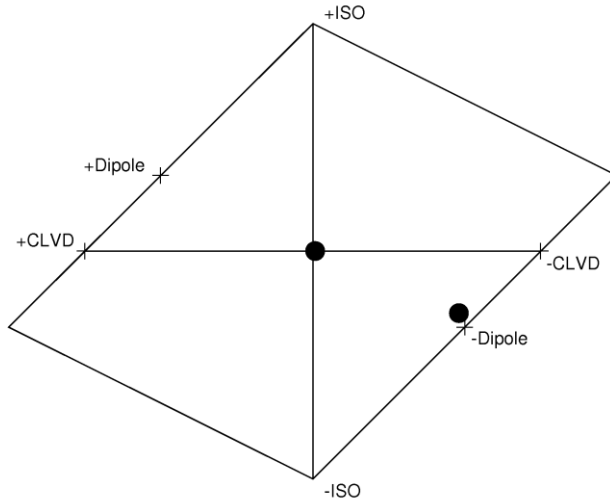


Figure 6 Hudson plot for displaying source components. The filled circles represent the source components of the two examples in 2.3.

3 Moment tensor representations: basic relations

A moment tensor representation is a formula to explain the theoretical relation between ground motions at the stations and the moment tensor at the source. This usually considers the dynamic ground motion and the wave radiation pattern in the far field. However, the theory also explains static and near field (near source) ground motions as well as source-generated strain and stress variations in the Earth. Knowing the moment tensor representation (the forward problem), \mathbf{M} can be obtained by inverting one or several of the observed field variables. Moment tensor inversion requires the availability digital time series of observed data, e.g. full seismograms or at least P and S phases, measured un-clipped on linear and predictable acquisition systems (e.g. calibrated systems), and the calculation or availability of accurate synthetic seismograms of the Earth (i.e. Green's functions, denoted by \mathbf{G}). Therefore, moment tensor inversion is more demanding from an observational and computational point of view.

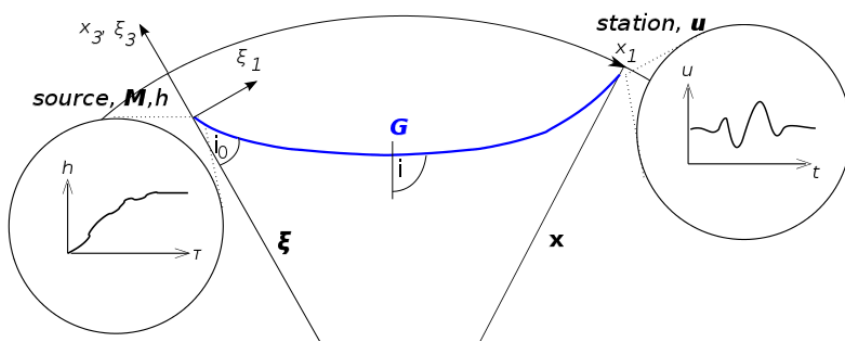


Figure 7 Geometry of the problem. The Green's tensor \mathbf{G} describes the impulse response of the Earth at station x_0 for a force excitation at ξ_0 . The point source is described by moment tensor \mathbf{M} and source time function $h(\tau)$. The ground motion at the station, $u(t)$, differs from the source excitation because of the filter effect of the Earth. The blue line indicates the ray path. The ray angle i is measured against the vertical; at the source i_0 defines the take-off angle. Note that the global coordinate system is source centered and that the 1-direction of both systems is defined by the source station path.

The basic theory and representation of seismic sources is outlined in chapter 3 of the NMSOP-2 and in IS3.1. We build on this theory and concentrate on the point source moment tensor representation of ground displacement (see equation 21 in IS3.1, neglecting the single force term)

$$u_n(\mathbf{x}, t) = M_{pq}(\boldsymbol{\xi}, t) * \frac{\partial}{\partial \xi_q} G_{np}(\mathbf{x}, \boldsymbol{\xi}, t)|_{\xi_0} = M_{pq}(\boldsymbol{\xi}, t) * G_{np,q}(\mathbf{x}, \boldsymbol{\xi}, t) \quad (14)$$

Equation (14) may alternatively be given in the frequency domain. The components of the ground displacement at location \mathbf{x} are declared by u_n . \mathbf{M} is the moment tensor of the seismic point source at location $\boldsymbol{\xi}$, and $G_{np,q}$ are spatial derivatives with respect to ξ_k of components of the Green's tensor \mathbf{G} . The Green's tensor can be viewed as a structural term defined between $\boldsymbol{\xi}$ and \mathbf{x} which describes all wave propagation effects including the elastostatic response of the Earth due to a single force delta-excitation at point $\boldsymbol{\xi}$ measured at point \mathbf{x} (Fig. 7). The first index of G_{np} gives the direction of the ground motion at the station, and the second index gives the direction of the force at the source. It is common practice to denote the two independent coordinate systems of the receiver (\mathbf{x}, t) and the source point $(\boldsymbol{\xi}, \tau)$ as independent variables in \mathbf{G} . Note that the following equivalence is used $G(\mathbf{x}, t; \boldsymbol{\xi}, \tau) = G(\mathbf{x}, t - \tau; \boldsymbol{\xi}, 0)$ (e.g., Aki and Richards, 2002). The components of the Green's tensors are often named Green's functions and may represent full seismograms. Later, we will introduce elementary seismograms as a special component of derivatives of the Green's tensor.

Equation (14) can be used to invert for moment tensors. Necessary condition is that observed seismograms have been deconvolved to ground displacement, velocity or acceleration (see IS11.1) and that Green's functions have been calculated between the source and receiver point assuming an appropriate Earth model. We will give examples of Green's function calculation below. Equation (14) can be written in matrix form, e.g. by considering the discrete form of the multichannel convolution integral (e.g., Krieger, 2011). We introduce notations \mathbf{d} , \mathbf{G}' and \mathbf{y} to indicate that the data and model vectors are not directly the tensor components defined in (14). They represent channels from more than one station (R is the maximal channel number), either in displacement, velocity or acceleration, and the derivatives or Green's functions. In the time domain, \mathbf{d} , \mathbf{G}' and \mathbf{y} further contain individual time samples (denoted by subscript index of time variables) at the different components and at different stations. We find

$$\begin{bmatrix} d_1(t_0) \\ d_2(t_0) \\ d_3(t_0) \\ \vdots \\ d_R(t_0) \\ d_1(t_1) \\ d_2(t_1) \\ \vdots \\ \vdots \end{bmatrix} = \begin{bmatrix} G'_{11}(t_0, \tau_0) & G'_{21}(t_0, \tau_0) & \dots & G'_{11}(t_0, \tau_1) & G'_{21}(t_0, \tau_1) & \dots \\ G'_{12}(t_0, \tau_0) & G'_{22}(t_0, \tau_0) & \dots & G'_{12}(t_0, \tau_1) & G'_{22}(t_0, \tau_1) & \dots \\ G'_{13}(t_0, \tau_0) & G'_{23}(t_0, \tau_0) & \dots & G'_{13}(t_0, \tau_1) & G'_{23}(t_0, \tau_1) & \dots \\ \vdots & \vdots & \ddots & \vdots & \vdots & \ddots \\ G'_{1R}(t_0, \tau_0) & G'_{2R}(t_0, \tau_0) & \dots & G'_{1R}(t_0, \tau_1) & G'_{2R}(t_0, \tau_1) & \dots \\ G'_{11}(t_1, \tau_0) & G'_{21}(t_1, \tau_0) & \dots & G'_{11}(t_1, \tau_1) & G'_{21}(t_1, \tau_1) & \dots \\ G'_{12}(t_1, \tau_0) & G'_{22}(t_1, \tau_0) & \dots & G'_{12}(t_1, \tau_1) & G'_{22}(t_1, \tau_1) & \dots \\ \vdots & \vdots & \ddots & \ddots & \ddots & \ddots \\ \vdots & \vdots & & & & \vdots \end{bmatrix} \begin{bmatrix} y_1(\tau_0) \\ y_2(\tau_0) \\ \vdots \\ y_6(\tau_0) \\ y_1(\tau_1) \\ y_2(\tau_1) \\ \vdots \\ \vdots \end{bmatrix}$$

or equivalently

$$\mathbf{d} = \mathbf{G}' \mathbf{y} . \quad (15)$$

Equation (15) is given in the form of a linear system of equations, and represents a discrete form of the multichannel convolution integral. \mathbf{d} and \mathbf{y} are the ‘data’ and ‘model’ vector, respectively, and \mathbf{G}' represents the coefficient matrix. Dimension of \mathbf{d} , \mathbf{y} and \mathbf{G}' are determined by the length of the data seismograms, the number of channels and the length of the assumed source time function (N_t), and can easily grow large. The data vector \mathbf{d} consists of individual seismograms measured at different stations. These may be full seismograms, usually band-pass filtered, or windowed traces of specific wave phases. The coefficient matrix \mathbf{G}' is build from derivatives of the Green’s functions (filtered and processed in the exact same way as the data). The components of the model vector \mathbf{y} contain the $6 \times N_t$ unknowns and are formed by holomorphic mapping of the moment tensor components into a model vector \mathbf{y} , e.g.

$$\begin{aligned} y_1 &= M_{11}, & y_2 &= M_{12}, & y_3 &= M_{22}, \\ y_4 &= M_{13}, & y_5 &= M_{23}, & y_6 &= M_{33}, \end{aligned} \quad (16)$$

Equation (15) is typically solved by the least squares (LS) inversion technique, either in the time domain (e.g. multichannel Wiener filtering described, e.g., in Wiggins and Robinson, 1965; Sipkin, 1982) or in the frequency domain (e.g. generalized inverse using singular value decomposition, e.g., Menke 1989).

The system (15) is over-determined, i.e. it has more independent equations (data) than unknowns, if for instance enough ground motion measurements are available from different distances and station azimuths, such that the azimuthal data coverage is sufficient to resolve the radiation pattern of the source. Also, the assumed source time duration should be much smaller than the length of the seismograms (or is parameterized by simple functions). Equation (15) is written for 27 independent components of the spatial derivatives of the Green’s tensor (3rd order tensor, i.e. 3x3x3 components) if three component seismograms are inverted. Green’s functions in this general formulation would consider near and far field terms. The time history of each moment tensor component is assumed to be independent. Altogether, this leads to a large number of unknowns, which are possibly difficult to resolve. Additionally, the choice of waves types selected (near field, far field, body wave phases, surface waves, etc.), the frequency range, the type of applied filters as well as the weighting scheme applied to the equations may influence the outcome of the inversion. Therefore, the equations implemented in practice are often modified in comparison to equation (15). For instance, the number of unknowns is reduced, e.g. by simplifying the time history of the moment tensor or by specifying the type of source mechanism (e.g. non-explosive). The number of Green’s functions is reduced by taking advantage of Earth model symmetries and/or by neglecting near field terms. Additionally, damping and linear or non-linear constraints may be considered. This leads to modified schemes and equations.

We discuss representations of the source time and moment rate function, the concept of joint inversion point source moment tensors and centroid locations, the simplified representation formulas for a layered Earth model and for the far field, formulas for amplitude spectra and specific representations if only body waves or peak amplitudes are used. Some words are given for the relative moment tensor inversion, the normal mode summation and how to calculate Green’s functions in practice.

3.1 Resolving the time dependency of moment tensors

The components of the moment tensor are time dependent and are related to the time history of slip (or rupture) at the source. Equation (15), or the equivalent form in the frequency domain, invert for the independent time function of each moment tensor component. The problem is often ill-posed and source-time functions vary a lot between the components. Different approaches have been suggested to stabilize the source time function inversion.

Often, a homogeneous rupture process is assumed, so that each moment tensor component has the same time history, e.g. $h(t)$. Then, it is useful to factorize the time history and leave only the magnitude of the time-independent scaling factors of the moment tensor components, e.g. denoted by \hat{M}_{pq} , leading to

$$M_{pq}(t) = h(t)\hat{M}_{pq} \quad \text{with} \quad h(t) = \begin{cases} 0 & \text{for } t \leq 0 \\ 1 & \text{for } t > T_d > 0 \end{cases} \quad (17)$$

where T_d is the duration of the ramp-like source time.

A common simplification is to use only far-field recordings. The far field displacement scales with the time derivative of h , i.e. $\dot{h} = dh/dt$, often denoted as moment rate function.

Near field Green's functions represent the component of the Green's functions, which remain zero at all times far from the source. Near and far field terms can be derived by equating the derivative of \mathbf{G} with respect to the source coordinate ξ_k , and separating the terms attenuating faster and slower. Lets assume ξ as independent variable. Both other intrinsic variables of G , x and $t-\tau$, depend on the distance to the source, which itself depends on ξ . The derivative of G is equated by

$$\frac{\partial}{\partial \xi_q} G_{np}(\mathbf{x}, t') = \frac{\partial G_{np}}{\partial x_l} \frac{\partial x_l}{\partial \xi_q} + \frac{\partial G_{np}}{\partial t} \frac{\partial t'}{\partial \xi_q} = G_{npq}^{(n)} + \dot{G}_{npq}^{(f)} . \quad (18)$$

t' is the retarded time at the station. For body waves, $\partial t'/\partial \xi_k$ are components of the slowness vector of the phase. The first and second term are associated with the near-field and far-field term of \mathbf{G} , associated by superscripts (n) and (f). Inserting (17) and (18) into (14) leads to the far field moment tensor representation as

$$u_n^{(f)}(\mathbf{x}, t) \approx \hat{M}_{pq} h(t) * \dot{G}_{npq}^{(f)}(\mathbf{x}, t) = \hat{M}_{jk} \dot{h}(t) * G_{npq}^{(f)}(\mathbf{x}, t) \quad (19)$$

Equation (19) shows that displacement in the far field depends on moment rate function and the far field Green's functions excited by a unit step at the point source. This is a general result, which explains that the far field body wave pulses from earthquakes are related to time derivatives of the source time function at the source. If the source time function is an ideal step function, the far field pulse is a pulse like. If it is a ramp function of duration T_d , the expected body wave pulse has the shape of a boxcar function of duration T_d .

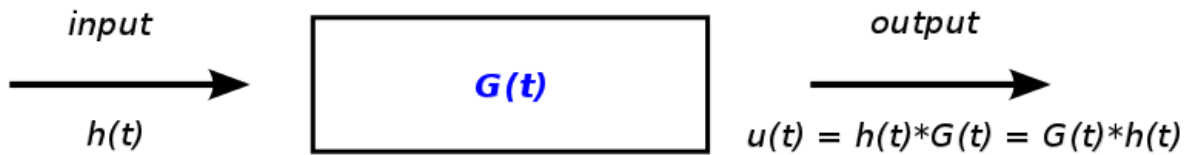


Figure 8 The Earth is described as a linear system with impulse response $G(t)$ (Green function). The ground motion response $u(t)$ at the station depends on $G(t)$ and the excitation $h(t)$ at the seismic source (input). The shape of the source radiation, i.e. the moment tensor, has been set unity in the 1D sketch (i.e. representing an explosive source as special case).

The interrelation between source time function $h(t)$ and displacement $u(t)$ can also be understood as a filtering effect (Fig. 8). $h(t)$ is the input signal. The linear filter is represented by $G(t)$ as the elastic response of the Earth. The ground displacement at the station, $u(t)$, is the filter output, and is equated as a convolution integral between the input and the filter.

Before we give some examples on how to estimate moment rate functions in practice, we use equation (19) to derive and explain the centroid time τ_0 . The centroid time is a point source parameter, defining the centre time of the wave radiation process. It is defined from the long period approximation of (19), which is valid if the period is $T > T_d$. A Taylors series expansion of the Green's tensor in (19) around the centroid τ_0 leads to

$$u_n^{(f)}(\mathbf{x}, t) \approx \hat{M}_{pq} G_{npq}^{(f)}(\mathbf{x}, t - \tau_0) + \hat{M}_{pq} \dot{G}_{npq}^{(f)}(\mathbf{x}, t - \tau_0) \int_0^\infty \dot{h}(\tau)(\tau - \tau_0) d\tau + \dots$$

The convolution integral is written in explicit form. The centroid time τ_0 is then defined in such a way that the integral on the right-hand side vanishes (see Fig. 9 and Nabelek, 1984). For low-pass filtered seismograms the other higher order terms can be omitted, which gives the temporal (and spatial) point source representation of ground displacement as

$$u_n^{(f)}(\mathbf{x}, t) = \hat{M}_{pq} G_{npq}^{(f)}(\mathbf{x}, t - \tau_0) . \quad (20)$$

Note that the far field displacements in (20), $u^{(f)}$, becomes zero a long time after waves have passed through the observing point since Green's functions in the far field are zero for large t .

Although equation (20) is appropriate if the seismograms are low-pass filtered, many authors try to resolve the time history $h(t)$ or, at least, the source duration. Although we have not yet strictly defined the spatial point source, we note that attempts to retrieve the source time functions of a spatial point source are not always useful. This is because a spatial point source moment tensor representation requires wavelengths larger than the size of the rupture plane. Resolving the source time is then only possible if the rise-time of the slip function at a single slip patch is longer than the rupture duration.

A common method to resolve the time dependency of $h(t)$ uses the linear representation in (15) and a two step inversion approach. Examples are given by Vasco (1989) or Cesca and Dahm (2007). The first inversion step estimates the independent time function of each

moment tensor component y_k . This may be performed either in the time or in the spectral domain. The second inversion step aims to retrieve the dominant common time history $h(t)$ presented in each component. A singular value decomposition of the matrix formed by the time dependent moment tensors is calculated. The matrix of orthogonal eigenvectors are weighted by the eigenvalues. The dominant time history common to all source components is then represented by the system of equations, which considers only the largest eigenvalue and sets all other eigenvalues to zero. More details can be found in e.g. Vasco (1989), Cesca and Dahm (2007) or Vavryczuk and Kühn (2012).

Other methods use smooth parameterizations of the moment rate function and solve directly the non-linear inverse problem for dh/dt (equation 19). The two most common parameterizations are a series of boxcars or overlapping triangles (e.g., Tsai et al., 2005, for the Great Sumatra-Andaman earthquake). The boxcar parameterization and the iterative, linearized least-squares inversion is described in, e.g., Tanioka and Ruff (1997) or Lay and Wallace (1995).

Tocheport et al. (2007) follow a different approach, which uses a stack of time-shifted and weighted body wave pulses at different stations minimized against an average source time function. The time shifts and weights are parameter of the inversion, which is solved by simulated annealing. Since the method requires isolated body waves, the method can only be applied to deep and intermediate earthquakes.

If a point source inversion is performed and seismograms are lowpass filtered, the details of the source time function of most earthquakes cannot be resolved. In such a case, often, only a rise time of the source time function is estimated (equivalent to the duration of a boxcar moment rate function, or other simple shapes). For instance, different rise times are tested in a grid search approach and the one leading to the least residuals in the waveform inversion is finally chosen (e.g., Heimann, 2011). The grid search approach can be used to determine station-related, apparent source durations after a best point source moment tensor is estimated. This may be of interest for a quick and rough analysis of rupture directivity, i.e. to separate fault and auxiliary plane and to distinguish the direction of rupture. For instance, Cesca et al. (2010b) suggest to keep the seismic moment and source mechanism of the point source solution and to invert for the source duration at each station. The apparent source time functions can then be interpreted in terms of a simplified kinematic rupture model. Zhang et al (2013) use an iterative deconvolution and stacking method to retrieve apparent source time functions for the purpose of rapid source imaging.

3.2 Representation of the centroid location (centroid moment tensor inversion)

Equation (20) was already defined for a centroid time τ_0 as origin time to calculate Green's functions. Similarly to the derivation of τ_0 spatial centroid coordinates ξ_0 can be derived by means of a Taylors series expansion of Green's functions. The problem is sketched in Fig. 9, a detailed derivaton can be found in, e.g., Nabelek (1984). Often, the hypocenter from the location of first phase arrivals is taken as a first approximation of the centroid. However, the hypocenter, which represents the point of rupture initiation (nucleation), may be tens or hundred kilometer away from the slip centroid if the earthquake was very large. Thus, the Green's functions calculated for the parameters of the hypocenter may be wrong or at least have large phase shifts relative to observed data. This may bias the moment tensor results. Three approaches are in use to reduce the possible bias.

The first workaround, instead of estimating a best centroid position, is to introduce ad hoc static phase shifts to the observed waveforms before inversion, for instance by cross correlation between observed and synthetic data. To first order the phase shifts may correct the mislocation of the centroid and leave the amplitudes of seismograms unchanged. However, the estimation of phase shifts is a tricky task and may easily lead to undesired (incorrect) shifts, especially if automatic processing is performed.

The more rigorous approach is to estimate the centroid during the inversion, which is named a centroid moment tensor inversion. The inverse problem has four additional unknowns (moment tensor components plus spatial and temporal coordinates) and becomes nonlinear. The centroid inversion can be setup similar to the Geiger method of a standard location (IS11.1). The nonlinear equations are approximated by the first linear terms of a Taylor series expansion around a starting solution. For instance, the hypocenter is used as starting location. The inversion for changes of source parameters is linear and solved employing a standard LS method. The solution is used to improve the starting solution, and the process is iteratively repeated until the changes become very small or the residuals are minimal. Since the equations for moment tensor inversion are linear, the moment tensor inversion itself is straight forward will always find an optimal solution. However, Green's functions have to be recalculated for the updated centroid location during each iteration. The centroid location problem is nonlinear and will have the same problems of non-uniqueness and non-convergence as standard earthquake location, especially since waveforms instead of first motions are fitted. In practice, depth centroid moment tensor inversion is thus often estimated by a grid search over a depth range in fixed steps combined with additional empirical static phase shifts at each station (limited to a fixed range of allowed phase shifts). Considering static phase shifts in addition to centroid depth location has the advantage that the impacts from incorrect Earth models or unaccounted 3D structure are reduced.

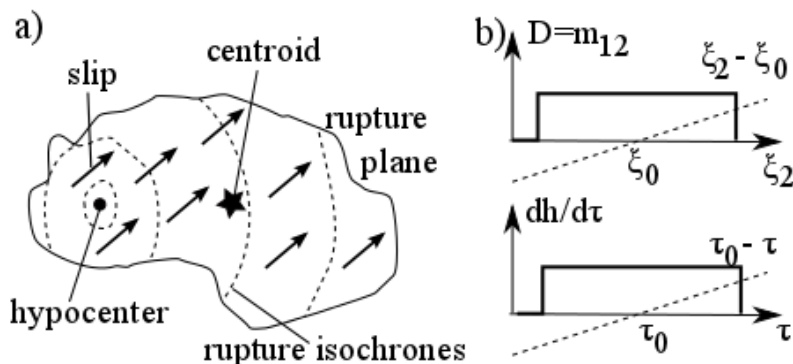


Figure 9 a) Schematic sketch of an earthquake rupture and the definition of hypocenter, centroid, rupture plane and slip. Rupture and slip is parameterized by the moment tensor density, m , and its time history $h(t)$. b) 1D visualization of spatial and temporal centroid coordinates to balance the third order spatial ($\int_V (\xi_k - \xi_{0k}) m_{ij} dV = 0$) and temporal moments ($\int_\tau (\tau - \tau_0) (dh/d\tau) d\tau = 0$) to zero (principle is comparable to finding the center of gravity).

The third approach to handle an unknown centroid location is to invert amplitude spectra in the first iteration. Amplitude spectra discard the phase information and are therefore less affected by incorrect centroid locations and Earth models. However, the amplitude spectra

cannot resolve the polarity of the source mechanism. This means an amplitude spectra inversion alone cannot resolve whether the seismic source was an explosion or an implosion, or whether the earthquake was a thrust or a normal faulting event. However, strike and dip of the fault and auxiliary planes are resolved. In order to resolve the polarity ambiguity either additional information is added to the inversion (e.g. first motion polarities), or the inversion is performed in a two-step approach, where amplitude spectra are inverted in the first iteration, and time-shifted full waveforms are considered in addition in a 2nd iteration. The 2nd step may keep strike and dip of the first solution fixed. We will further discuss this third approach below.

3.3 Representation in a layered Earth model

If a layered Earth model is assumed, only 10 instead of 27 Green's functions are needed. If additionally only far field seismograms (see IS3.1) are analyzed, the number of required Green's functions is further reduced to 8. If only body wave phases are inverted (ray-theoretical description), the number of Green's functions further reduces to 3 greatly simplifying the inverse problem. The reduced set of specific Green's functions are often combinations of the original Green's functions defined under specific azimuth angles and are called elementary seismograms. We briefly outline the redundancy of Green's tensors and the definition of elementary seismograms.

Fig. 7 indicates two coordinate systems, a local one defined at the source location and a global one for the source-station geometry. Sensor components of seismometers are usually measured in an east–north–up system. The sensor components in the representation formulas and in Fig. 7 should be defined in the curvilinear, global source-centered system, e.g. by radial, transversal and down directions (distance r , azimuth φ and depth z). However, the moment tensor is usually defined for a local Cartesian system. At the pole, the local NED system, with $x=N$, $y=E$ and $z=\text{down}$, has the same directions as the local spherical system. Only in the specific case where the great circle path between source and receiver is along a meridian, i.e. the station is under azimuth $\varphi'=0$, the local and global directions would be identical. We denote the Green's tensor in this specific case by \mathbf{G}^0 . If the media is invariant to azimuthal rotations around z , e.g. layered Earth models, the Green's tensor can be given as a rotated version of \mathbf{G}^0 . We define unprimed and primed indices to define the unrotated (NED) and rotated azimuth directions. $R(\varphi')$ declares a matrix describing rotation with angle φ' around the z direction. Using tensor rotation the Green's tensor in the source-station system can be equated from \mathbf{G}^0

$$G_{n'p',q'} = R_{p'p}(\varphi') R_{q'q}(\varphi') G_{n'p,q}^0 = R_{p'p}(\varphi') G_{n'p,q}^0 R_{qq'}(-\varphi') . \quad (21)$$

At $\varphi'=0$ the P-SV motion can only be excited by moment tensor components M_{xx} , M_{zz} , M_{xz} , M_{zx} and M_{yy} (note that M_{yy} comes into play only for near field displacements). Contrary, SH motion can only be excited by moment tensor components M_{xy} and M_{yx} . This reduces the zero azimuth tensor to

$$\mathbf{G}_r^0 = \begin{pmatrix} G_{rx,x}^0 & 0 & G_{rx,z}^0 \\ 0 & G_{ry,y}^0 & 0 \\ G_{rz,x}^0 & 0 & G_{rz,z}^0 \end{pmatrix}$$

$$\mathbf{G}_\varphi^0 = \begin{pmatrix} 0 & G_{\varphi x,y}^0 & 0 \\ G_{\varphi y,x}^0 & 0 & G_{\varphi y,z}^0 \\ 0 & G_{\varphi z,y}^0 & 0 \end{pmatrix}$$

$$\mathbf{G}_z^0 = \begin{pmatrix} G_{zx,x}^0 & 0 & G_{zx,z}^0 \\ 0 & G_{zy,y}^0 & 0 \\ G_{zz,x}^0 & 0 & G_{zz,z}^0 \end{pmatrix}$$

Thus, in layered media, equation (14) reduces to

$$\begin{aligned}
 u_{r'} &= +g_1 \star (M_{xx} \cos^2 \varphi + M_{yy} \sin^2 \varphi + M_{xy} \sin 2\phi) \\
 &\quad + g_9 \star ((M_{xx} \sin^2 \varphi + M_{yy}) \cos^2 \varphi - M_{xy} \sin 2\phi) \\
 &\quad + g_2 \star (M_{xz} \cos \phi + M_{yz} \sin \phi) \\
 &\quad + g_3 \star M_{zz} \\
 u_{\varphi'} &= +g_4 \star \left(\frac{1}{2} (M_{yy} - M_{xx}) \sin 2\varphi + M_{xy} \cos 2\varphi \right) \tag{22} \\
 &\quad + g_5 \star (M_{yz} \cos \varphi - M_{xz} \sin \varphi) \\
 u_{z'} &= +g_6 \star (M_{xx} \cos^2 \varphi + M_{yy} \sin^2 \varphi + M_{xy} \sin 2\phi) \\
 &\quad + g_{10} \star ((M_{xx} \sin^2 \varphi + M_{yy}) \cos^2 \varphi - M_{xy} \sin 2\phi) \\
 &\quad + g_7 \star (M_{xz} \cos \phi + M_{yz} \sin \phi) \\
 &\quad + g_8 \star M_{zz}
 \end{aligned}$$

with the following elementary seismograms

$$\begin{aligned}
 g_1 &= G_{r'x,x}^0 & g_2 &= G_{r'x,z}^0 + G_{r'z,x}^0 & g_3 &= G_{r'z,z}^0 \\
 g_4 &= G_{\varphi'x,y}^0 + G_{\varphi'y,x}^0 & g_5 &= G_{\varphi'y,z}^0 + G_{\varphi'z,y}^0 \\
 g_6 &= G_{z'x,x}^0 & g_7 &= G_{z'x,z}^0 + G_{z'z,x}^0 & g_8 &= G_{z'z,z}^0 \\
 g_9 &= G_{r'y,y}^0 & g_{10} &= G_{z'y,y}^0
 \end{aligned} \tag{23}$$

Equation (22) and (23) represent the system of equations for a layered Earth. Only ten independent elementary seismograms $g_1 - g_{10}$ are needed, of which components g_9 and g_{10} contain only near field terms (e.g. Müller, 1985) and are neglected in most moment tensor studies of earthquakes.

3.4 Representation for body waves (peak amplitudes and amplitude ratios)

The number of independent Green's functions is further reduced if a ray theoretical approximation is valid, for instance, if we consider only far field body wave phases associated with a specific ray path (e.g., qP and qS phases). The ray direction (ray angle i , see Fig. 7), is related to the horizontal and vertical components of the slowness vector by

$$(s_x, s_y, s_z) = (s_x, 0, s_z) = |s| (\sin(i), 0, \cos(i)). \quad (24)$$

If we consider in the far field that $M_{pq}(\xi_0) * G_{np,q}(x, \xi_0) \approx dM(\xi_0)/dt * G_{np}(x, \xi_0) s_q + O(\text{near field terms})$ (e.g. Dahm, 1996), the rotation of the zero azimuth Green's tensor leads to further simplified moment tensor representation for the three modes of body waves phases:

for qP

$$\begin{aligned} G_{z'x}^0 s_x &= g_6 = I_e^P \sin^2 i \\ G_{z'x}^0 s_z + G_{z'z}^0 s_x &= g_7 = I_e^P 2 \sin i \cos i \\ G_{z'z}^0 s_z &= g_8 = I_e^P \cos^2 i, \end{aligned}$$

for qSV

$$\begin{aligned} G_{r'x}^0 s_x &= g_1 = I_e^{SV} \cos i \sin i \\ G_{r'x}^0 s_z + G_{r'z}^0 s_x &= g_2 = I_e^{SV} (\cos^2 i - \sin^2 i) \\ G_{r'z}^0 s_z &= g_3 = -I_e^{SV} \sin i \cos i, \end{aligned} \quad (25)$$

and for qSH

$$\begin{aligned} G_{\phi'x}^0 s_y + G_{\phi'y}^0 s_x &= g_4 = I_e^{SH} \sin i \\ G_{\phi'y}^0 s_z + G_{\phi'z}^0 s_y &= g_5 = I_e^{SH} \cos i, \end{aligned}$$

where I_e^P , I_e^{SV} and I_e^{SH} now define elementary wave mode phases (e.g. seismogram wavelets containing specific body wave phases) which consider the geometrical divergence, the attenuation and the travel time of the phase along the ray path between source and receiver. Note that $G_{\phi'x}^0 s_y = 0$ and $G_{\phi'z}^0 s_y = 0$ (see Dahm, 1996). Insertion in equation (14) leads to (see also Box 9.13 in Aki and Richards, 2002)

P wave:

$$\begin{bmatrix} u_{r'}^P \\ u_{z'}^P \end{bmatrix} = \begin{bmatrix} (I_e^P)_{r'} \\ (I_e^P)_{z'} \end{bmatrix} * \left[\begin{array}{l} [(M_{xx} \cos^2 \varphi + M_{yy} \sin^2 \varphi + M_{xy} \sin 2\phi) \sin^2 i \\ + (M_{xz} \cos \phi + M_{yz} \sin \phi) 2 \sin i \cos i \\ + M_{zz} \cos^2 i] \end{array} \right]$$

SV wave:

$$\begin{bmatrix} u_{r'}^{SV} \\ u_{z'}^{SV} \end{bmatrix} = \begin{bmatrix} (I_e^{SV})_{r'} \\ (I_e^{SV})_{z'} \end{bmatrix} * \left[\begin{array}{l} [(M_{xx} \cos^2 \varphi + M_{yy} \sin^2 \varphi + M_{xy} \sin 2\phi) \sin i \cos i \\ + (M_{xz} \cos \phi + M_{yz} \sin \phi) (\cos^2 i - \sin^2 i) \\ - M_{zz} \sin i \cos i] \end{array} \right] \quad (26)$$

SH wave:

$$u_{\varphi'}^{SH} = (I_e^{SH})_{\varphi'} * \left[\begin{array}{l} \left(\frac{1}{2} (M_{yy} - M_{xx}) \sin 2\varphi + M_{xy} \cos 2\varphi \right) \sin i \\ + (M_{yz} \cos \varphi - M_{xz} \sin \varphi) \cos i \end{array} \right]$$

Note that for each body wave phase of qP, qSV or qSH type only one elementary “phase-wavelet” enters the moment tensor representation. Equation (26) forms the basis for the well known polarity method, where for each phase only the polarity is considered to constrain the focal solution of a double couple source (see chapter 3). It is also the basis for a moment tensor inversion based on generalized rays (e.g. Nabelek, 1984), peak amplitude (e.g. Ebel and Bonjer, 1990), and amplitude ratios or the relative moment tensor inversion (e.g. Dahm, 1996).

Equation (26) can be used for body wave peak amplitude moment tensor inversion of weak and moderate events with short source duration. For instance, peak amplitudes or waveform moments (=displacements integrated over the first pulse) of low pass filtered P and S phases may be measured and used as input data for inversion. Low pass filtering with a passband below the corner frequency of the event has to be performed to avoid amplitude distortion from rupture directivity. Seismograms need to be deconvolved to ground motion to estimate true seismic moments. The geometrical ray parameters, i.e. the ray azimuth and take-off angle, are typically taken from a location program where ray tracing is performed. Although elementary seismograms I_e are reduced to a scalar factor comprising geometrical and intrinsic attenuation, and therefore might be estimated by ray tracers during location, it is recommended to extract I_e from complete synthetic seismograms which are filtered in the same way as the observed seismograms. This may avoid bias from apparent polarity flipping, a problem that may occur if short period stations were used. The method has been used occasionally for short period local and teleseismic earthquakes studies but is now of lesser relevance since broadband data are often available. Data problems were often difficult to identify since observed and synthetic waveforms were not directly compared. In order to further stabilize the method, pure double couple constraints (shear crack constraints) can be introduced.

A derivative of the peak amplitude method is the amplitude ratio method to determine focal solutions for double couple sources. Amplitude ratios between P, SV and SH phases are used as input data, together with P phase polarities, and the associated relations between the

elementary seismograms I_e of the different wave modes are considered from ray theory. A commonly used Fortran package is *focmec* (by A. Snoker, see <http://www.iris.edu/pub/programs/focmec>).

3.5 Relative moment tensor inversion using multiple events (body wave method)

To locate earthquakes multiple event inversions were developed. Well-known examples are the joint hypocenter, the master event location and the hypoDD methods (IS11.1). A moment tensor approach similar to the master event location was developed by e.g. Dahm (1996). The method is of interest if earthquake clusters are analyzed. Spatially clustered seismicity may occur for example during aftershock sequences, for earthquakes swarms in volcanic and geothermal areas, or at specific structures at tectonic faults or subducted plates (e.g., deep earthquake clusters). The concept of the relative moment tensor inversion is to use a reference mechanism (reference event) from the cluster, which is fixed during inversion, and to estimate the moment tensors of the studied events relative to the reference event. Since the studied and the reference earthquake from a tiny cluster have similar elementary seismograms I_e , the I_e factors can be eliminated from equation (26). Geometrical and intrinsic attenuation, amplification from site effects or unknown instrument functions have thus no or only a minor influence on the moment tensor result. The method is further described in Dahm (1996) and Dahm and Brandsdottir (1997). Necessary pre-requisites for application are that

- (a) the mechanism of the reference event is known a priori,
- (b) the events are tightly clustered and seismograms are low-pass filtered, so that events can be regarded as temporal and spatial point sources within approximately one wavelength from the reference event,
- c) seismograms are low-pass filtered prior to measuring peak amplitudes. The corner frequency of the low-pass filter should be in the range of the corner frequency of the largest studied event of the cluster (potentially limiting the size of the smallest event that can be analyzed).

Dahm (1996) describes an extension of the method, for which the necessity of a fixed reference mechanism can be dropped when the radiation patterns within the earthquake cluster differ sufficiently.

3.6 Full waveform method using amplitude spectra

Full waveform methods considering broadband seismograms are nowadays routinely in use to study moderate and strong earthquakes at regional and teleseismic distances. As discussed in the previous paragraphs unconsidered phase shift between Green functions and data may be present if the centroid coordinates are incorrect or if the Earth model to calculate Green's functions is too simplified. Amplitude spectra inversions neglect the phase information. In the frequency domain, equation (15) can be written as

$$\tilde{d}(\omega) = \tilde{G}'_{nk}(\omega) y_k(\omega) = [\text{Re}\{\tilde{G}'_{nk}\} + j\text{Im}\{\tilde{G}'_{nk}\}] y_k , \quad (27)$$

where $\text{Re}\{\}$ and $\text{Im}\{\}$ are the real and imaginary part of the complex spectrum and j is the imaginary unit. The absolute value of the spectral seismogram amplitudes are then

$$|\tilde{d}| = \left[(\text{Re}\{\tilde{G}'_{nk}\}y_k)^2 + (\text{Im}\{\tilde{G}'_{nk}\}y_k)^2 \right]^{1/2} = f(\tilde{G}', y) . \quad (28)$$

The amplitude spectrum (28) is a non-linear function f of the moment tensor components y . The problem can be linearized and solved by an iterative inversion scheme (e.g., the gradient method). Equation (28) is linearized by means of the linear term of a Taylors series expansion around a starting moment tensor solution. During each iteration, changes of moment tensor components are solved by minimizing the residual data vector. Local minima can be easily avoided if different starting models are considered by means of a grid search, e.g. represented by double couple starting solutions with different orientations. Examples are provided in e.g. Dahm et al. (1999 and Cesca et al. (2006).

Amplitude spectra inversion is in generally more robust and independent of phase misalignments as long as the time windows taken for inversion contain the phases modeled by Green's functions. The most serious drawback of amplitude spectra inversion is that the polarity of the source mechanism is not used resulting in a set of two indistinguishable moment tensor solutions with common nodal planes but different polarities. Therefore, amplitude spectra inversion is often implemented as a first step inversion, which is refined in a second step by considering additional constraints. For instance, polarity information of first onsets of body wave phases may be used to resolve the polarity ambiguity. A more elegant waveform approach is to use the results from the first inversion to estimate phase shifts at selected high quality stations, e.g. by means of cross correlation between observed and predicted waveforms, and to add these time domain traces in a second inversion step (e.g. Heimann, 2011; Cesca et al., 2010). The second step may either use time traces of phase corrected waveforms only or may be run as a weighted mixed input inversion considering amplitude spectra at all stations and time traces at selected key stations only. Since computation time and memory is not an issue any more we recommend the two-step inversion, which can easily be automated and reduces the problem of misaligned phases due to incorrect Earth models or earthquake locations.

3.7 Moment tensor representation using eigen-vibrations and eigen-modes of the Earth

The moment tensor representation calculates ground displacement as a sum of weighted Green functions (elementary seismograms), where weights are represented by moment tensor components. How the Green's functions are calculated is not specified. Most often, surface or body waves are used for moment tensor inversion. Body and surface waves in any finite body can be understood as a sum over a large number of eigen vibrations of this body. Therefore, Green's functions and synthetic seismograms may be calculated by summing up normal modes of the Earth. Such an approach was used by the first systematic global centroid moment tensor program led by A. Dziewonski in the early 1980's at Harvard University inverting fundamental modes and long period surface waves (> 135 s). Other types of representation formulas may be derived for the normal mode theory, which are not further specified here (see, e.g., Dahlen and Tromp, 1998). Normal mode theory, for a long time, has been the most complete approach to calculate synthetic seismograms and Green's functions, since self gravitation, Earth rotation, Earth ellipticity and pre-stress are all included.

3.8 Codes to calculate Green functions for moment tensor inversion

Depending on the mode and type of selected data different computer codes can be recommended to calculate synthetic Green functions. The list below is incomplete and represents a selection based on the author's experience.

Table 2 Computer codes to calculate synthetic seismograms

| Input data | Type of code | Name of code | Link, reference |
|---|--|-----------------------|--|
| Local and regional full waveforms (body and surface waves), high frequencies. | Reflectivity, layered Earth models, anisotropy & intrinsic attenuation, receiver at depth | Qseis (fortran code) | Wang (1999), ftp://ftp.gfz-potsdam.de/pub/home/turk/wang/qseis2006-code+input.zip |
| Global and regional full waveforms | Numerical integration of the SODE (integration of minors) | GEMINI (fortran code) | Friederich and Dalkomo (1995), http://www.quest-itn.org/library/software/gemini-greens-function-of-the-earth-by-minor-integration |
| Global and regional full waveforms, free oscillations, tsunami, infrasound | Hybrid method (analytical and numerical integration) for layered Earth models. self gravitation, ocean layer, atmospheric layer, Earth normal modes, long time series. | QSSP (fortran code) | Wang, R. (1997), ftp://ftp.gfz-potsdam.de/pub/home/turk/wang/qssp2010-code+input.rar |
| Free oscillations, long period surface waves | Numerical integration, layered Earth models, self gravitation, anisotropy, attenuation. | MINEOS (fortran) | http://www.geodynamics.org/cig/software/mineos |
| Full waveforms | Numerical approach, 3D Earth models, ellipticity, rotation, self gravitation, attenuation. | SPECFEM3D | http://www.geodynamics.org/cig/software/specfem3d-globe |

Green's function can be pre-calculated for specific Earth models (e.g. standard models) and stored in Green's function databases. They can then be shared over the internet, e.g. on the KINHERD web page (<http://kinherd.org>), from where they can be downloaded by users, for instance if computing power or facilities are not available to build own databases. Exercise EX 3.6 gives an example, referring to moment tensor inversion based on the Pyrocko package (<http://emolch.github.com/pyrocko>) or the Kiwi Tools (<http://kinherd.org/kiwitools>) (e.g. RAPIDINV, see <http://kinherd.org/rapidinv>), which can directly use these pre-calculated databases.

4 Moment tensor inversions schemes in practice

Solving equation 3 in the time or in the frequency domain includes several steps from data preparation and Green's function calculation to solving a system of linear equations. The reliability and evaluation of the outcome, i.e. a moment tensor, depends not only on the datasets and a formal error estimation but on many additional factors, where the most important are listed below.

1) Data acquisition and pre-processing

- selection of seismograms with good signal-to-noise ratio
- unclipped signals
- good azimuthal coverage
- removing mean value and linear trends, detection of data gaps
- correcting for instrument response, converting seismograms to displacement, velocity or acceleration
- selection of waveforms, e.g., P, S and surface wave windows or full seismograms
- low-pass filtering appropriate to the dataset to remove high-frequency noise and estimating the corner frequency of the source to safely satisfy the point source approximation

2) Calculation of accurate synthetic Green functions for specific

- earth model
- location of the source
- receiver position

3) Inversion and interpretation of the inversion result

- decision for an inversion algorithm to solve eq. 3 or eq. 12
- test of resolution for all free parameters of the source model
- decomposition of the moment tensor, e.g., into best double couple plus CLVD

The inversion may be performed in the time or frequency domain either using a singular value decomposition to calculate the generalized inverse matrix or, e.g., by LU decomposition. We do not provide details: the reader may find more information and software in Press et al. (2007) (chapter 2, especially 2.3). A general introduction and overview on data inversion can be found in the textbooks of Menke (1989) and Aster et al. (2013). Linearization and iterative solution strategies using one specific or a set of start models are required for instance to solve eq. 12 (amplitude spectra based solution).

Care must be taken to match the synthetic and observed seismograms. Alignment of observed and synthetic waveforms is facilitated by cross-correlation techniques. In most moment-tensor inversion schemes, focal depth is assumed to be constant. The inversion is done for a range of focal depths and the best solution is assumed to be the with the lowest misfit.

Dufumier and Cara (1995) and Dufumier (1996) give a systematic overview for the how M_{ij} results are affected by differences in the azimuthal coverage and by using only P waves, P plus SH waves or P and SH and SV waves for the inversion with body waves. Their results indicate the most important factor is good azimuthal coverage, followed by the combined use of P and S phases (and Love and Rayleigh waves). A systematic overview with respect to the effects caused by an erroneous velocity model for the Green function calculation and the

effects due to wrong hypocenter coordinates can be found in Šilený et al. (1992), Šilený and Pšenčík (1995), Šilený et al. (1996) and Kravanja et al. (1999).

The dynamical boundary conditions on the solid free surface imply that the moment tensor elements M_{xz} ($= M_{13}$) and M_{yz} ($= M_{23}$) vanish as the source location approaches the Earth's free surface or the seafloor. As a result, these vertical dip-slip components are not well constrained for shallow-focus sources. A discussion regarding the related uncertainties for the determination of focal mechanisms, the centroid depth but also the scalar seismic moment can be found in Bukchin et al. (2010).

Depending on the dataset the isotropic component, M_{iso} , may be difficult to resolve. Therefore, an isotropic component with strength of less than 10% of the strength of the full moment tensor is often considered to be insignificant. A better approach is to test the statistical significance, e.g. by means of an F-test.

Significant CLVD components are often reported for large intermediate-depth and very deep earthquakes. In many cases, however, it can be shown that these may be caused by the superposition of several sub-events with different double-couple mechanisms (Kuge and Kawakatsu, 1990; Frohlich, 1995; Tibi et al., 2001).

How good is a specific solution? Several standard approaches exist to get an answer to this question. The numerical stability of the inversion can, for instance, be checked with the condition number. This number is defined as the ratio between the square root of the largest eigenvalue to the smallest eigenvalue of the generalized inverse and is an outcome of calculating the generalized inverse using a singular value decomposition method. It indicates the overall sensitivity of the solution to errors in the data. For iterative inversion schemes straightforward error estimation techniques are not applicable. One way to estimate the errors in the solutions is the use of many start models within reasonable limits and subsequent evaluation of the scatter in the resulting model parameters. Jackknifing and bootstrapping (see, e.g., Shao and Tu, 1995) are also widely used methods to test the stability of solutions, especially when non-linear iterative schemes are used (e.g., Heimann, 2011; Zahradník and Custódio, 2012). See also Valentine and Trampert (2012) for a recent assessment of uncertainties for centroid moment tensor determinations.

5 Free software packages for moment tensor inversion

Here we list freely available software packages for moment tensor inversion. We mention briefly differences regarding the distance range and details of the inversion outcome.

- RAPIDINV (Cesca, 2010), based on the Kiwi Tools (Heimann, 2011): Time and frequency domain inversion code in the regional and teleseismic distance range using full waveform Green's function databases. Includes inversion for point source, simple finite sources and extensive resolution testing, see <http://kinherd.org/rapidinv> and exercise 3.6 of the NMSOP-2: „A practical in moment tensor inversion using the Kiwi tools“ (<http://gfzpublic.gfz-potsdam.de/pubman/item/escidoc:130023:6>)
- VOLPIS (Cesca and Dahm, 2007). A stand-alone frequency domain inversion code (fortran) for the study of time-dependent source parameters for long period volcanic

signals. Single forces and dipole forces (moment tensors) can both be inverted (<http://kinherd.org/volpis>).

- Time-Domain Moment Tensor INVerse Code (TDMT-INV) by Dreger (2003), for a description and software download see www.orfeus-eu.org/pub/software
- Regional moment tensor inversion code together with tutorial and examples by B. Herrmann see www.eas.slu.edu/eqc/eqccps.html
- ISOLA-GUI which is a matlab GUI for regional moment tensor inversion written by J.Zahradník and E. Sokos, see <http://seismo.geology.upatras.gr/isola>
- mtinvers (Dahm et al., 2007) is a stand-alone fortran code for regional and teleseismic point source inversion. Inversion can be constrained to opening/closing cracks, double couple source, shear source (<http://kinherd.org/mtinvers>).
- Mtinv package written by C. Ammon and G. Randall for point source moment tensor inversion in time domain in the regional distance range, see <http://eqseis.geosc.psu.edu/~cammon>
- MT5 package (McCaffrey et al., 1991) is a PC based software package for the inversion of teleseismic body waves for moment tensor solutions or double couple fault plane solutions, see <http://ees2.geo.rpi.edu/rob/mt5> and can also be found in the IASPEI Software Library, number 4.

Differences between the available packages arise from the implementation of constraints in the inversion either to stabilize the solution or for special purposes. As was mentioned in the subsection on problematic sources and moment tensor decomposition it is for many problems desirable to constrain the moment tensor to its deviatoric part by setting the trace of the moment tensor equal to zero. In this case only 5 moment tensor elements are left and the corresponding linear equation system can be found by recombining terms in the Eqs.s (3) and (6,7). This problem is still a linear one. Other constraints used are: double couple, tensile crack or a mixed situation. In these cases the inversion becomes non-linear and iterative inversion schemes have to be used.

The offered codes differ in several aspects. In the teleseismic distance range differences arise mainly regarding the computation of full wavefield Greens functions and the use of complete seismograms and/or if the inversion is performed for specific body wave phases like P and S and if surface waves are included. Here again an important detail is if the flat Earth transformation (Chapman 1973; Müller, 1977; Bhattacharya, 1996) is used to account for the sphericity of the Earth or if full wavefield Green's functions are calculated directly for the spherical Earth or if normal modes are used (see chapter 2.5 for freely available codes for the computation of full wavefield Green's functions).

In the regional distance range more codes are available to calculate full wavefield synthetics for layered media. The use of a regionally valid velocity model is critical (e.g. Donner et al., 2013). It should be mentioned that many velocity models used for location may show problems when used to produce longperiod surface waveforms because they may have been tuned to fit the crustal and upper mantle P-wave velocities not the S-wave velocities in the uppermost crustal layers.

Some codes use a full grid search regarding centroid time, centroid location and centroid depth: most codes at least search for a best fitting centroid depth.

Exercise EX 3.6 of the NMSOP-2 (DOI: 10.2312/GFZ.NMSOP-2_EX_3.6) provides a tutorial on how to setup Green's function databases and the MT inversion by using the Kiwi Tools.

6 Moment tensor catalogues

In the late 1970s and early 1980s the group headed by A. Dziewonski at Harvard University began routine determination of the seismic source parameters of all earthquakes with magnitude ≥ 5.5 using the centroid moment tensor (CMT) method (Dziewonski et al., 1981). This inversion tries to fit simultaneously the very long-period body wave train from the P arrival until the onset of the fundamental modes and mantle waves with periods longer than 135 s using synthetics produced by normal mode summation (see chapter 2.6). In addition the best point-source parameters (centroid epicentral coordinates, centroid depth and origin time) and the six independent moment tensor elements were published.

The Harvard group maintained, from 1981 to 2006, an extensive catalog of centroid moment-tensor (CMT) solutions for strong (mainly $M \geq 5.5$) earthquakes since 1976. This catalog is now maintained and continued by the Global Centroid Moment Tensor Project at Lamont-Doherty Earth Observatory (LDEO) of Columbia University. Their solutions, as well as quick CMT solutions of recent events, down to moment magnitudes $M_w \approx 4.5$ can be viewed at <http://www.globalcmt.org>. The products are also distributed by IRIS (see <http://www.iris.edu/spud/momenttensor>) and other data centers like the USGS. Harvard CMT solutions for the very largest, gigantic earthquakes (e.g., M_w 9.3 Sumatra, 26 December 2004) turned out to be systematically deficient (Stein and Okal, 2005; Tsai et al., 2005), and provisions have now been made to use longer periods for mega earthquakes.

As mentioned above the CMT inversion procedure seeks a solution for the centroid location of the earthquake. This centroid location may, for very large earthquakes, significantly differ from the hypocenter location based on arrival times of the first P-wave onsets. This initial hypocenter location corresponds to the place where rupture started. Therefore, the offset of the centroid location relative to the hypocentral location gives a first indication on fault extent and rupture directivity. In the case of the August 17, 1999 Izmit (Turkey) earthquake the centroid was located about 50 km east of the P-wave hypocenter. The centroid location coincided with the area where the maximum surface ruptures were observed.

Several institutions publish in recent years moment tensors determined using the W-phase (Kanamori, 1993; Kanamori and Rivera, 2008; Duputel et al., 2012). The ultra-longperiod W phase follows direct P on very broadband seismograms. Its use has the advantage to provide correct spectral levels for scalar moment determination also for slow ruptures what is important due to their high tsunami potential. See eost.u-strasbg.fr/wphase for a description of the method, the catalog and a list of further publications.

Several other institutions offer regularly moment tensor solutions. The following list is not complete and what is described may change in detail.

One of the most complete regional archives is published by Berkeley Seismological Laboratory (BSL) for Northern California based on inversion of full waveform synthetics mainly of mid- and longperiod surface waveforms (Dreger and Helmberger (1993) and Dreger (2003). The catalog reaches back till 1993. More references to methodological work and example cases can be found on the webpage seismo.berkeley.edu/mt.

Another regional catalog for Southern California is published by the Southern California Earthquake Data Center (SCEC) since 2000 and can be found at <http://www.data.scec.org>.

GEOAZUR-SCARDEC method. GEOAZUR offers near realtime moment tensor solutions for larger worldwide events using a body wave deconvolution method (Vallee et al., 2011).

An estimate for a point source source time function and plots showing the fit of synthetics and observed waveforms for P and SH are provided.

See <https://geoazur.oca.eu/spip.php?article1236>

GFZ worldwide moment tensor solutions are distributed since 2011. Solutions are based on a modification of the code of Dreger and Helmberger (1993) and Dreger (2003) and are given in text or graphical form. A catalogue can be found at <http://geofon.gfz-potsdam.de/eqinfo/list.php?mode=mt>

A fully automatic global moment tensor catalogue, since 2012, is provided by GFZ using the Kiwi Tools package. Uncertainties are evaluated using bootstrapping methods. Kinematic source solutions of the extended source are calculated for selected events (see Heimann, 2011). Catalogue can be found under <http://kinherd.org/quakes/>

The National Observatory of Athens (NOA) provides fast moment tensor solutions for events in the Mediterranean Sea region down to a magnitude of about Mw 3.5. The ISOLA software (Sokos and Zahradník, (2008, 2013). is used and a grid search to find the best centroid parameters is performed. Plots showing the fit of the synthetics to the waveforms are provided. See also

<http://bbnet.gein.noa.gr/HL/seismicity/moment-tensors>

INGV uses the Dreger (2003) time domain method to invert for moment tensors of earthquake in Italy and the surrounding regions. Solutions are provided in form of pdf files showing moment tensor solutions in text and graphical form. The quality of the solution can be judged from the fit of longperiod synthetic and data waveforms together with maps showing the azimuthal distribution of stations. See <http://cnt.rm.ingv.it/dmt.html>

INGV Bologna provides a different catalog for earthquakes larger than Mw 4.0 for events in Italy and larger than Mw 4.5 for events in the wider region based on an adaption of the centroid moment tensor method to model mid-period surface waves (Pondrelli et al, 2006, 2011). Solutions since 1976 are provided in text and graphical form.

The SED/ETHZ provides an automatic regional moment tensor catalogue for the entire European-Mediterranean region. Until 2010 the method was based on Braunmiller et al. (2002) and Bernardi et al. (2004). The reviewed catalog covers 1999 to 2006, the automatic MT catalog 2002-2010 (see <http://www.seismo.ethz.ch/prod/tensors/index>). The current regional MT determination covers Switzerland and vicinity and is based on the Dreger code and is described in Clinton et al., 2006).

Regional moment tensor solutions for Spain and its surroundings are provided by IGN, see e.g. <http://www.ign.es/ign/layoutIn/sismoPrincipalTensorZonaAnio.do>

Solutions are provided in text (Spanish language) and graphical form. A number for the variance reduction and waveform fits are provided.

The USGS provides several types of moment tensor solutions. The „fast“ moment tensor solutions are based on body wave inversion only. The USGS centroid moment tensors are resulting from longperiod full waveform inversion. Additionally the USGS publishes W-phase moment tensors from inversion of the ultra-longperiod W phase following direct P on very broadband seismograms. The latter has the advantage to provide correct spectral levels

for scalar moment determination also for slow ruptures important due to their tsunami potential. See the USGS homepage (in the moment under reconstruction)

An interesting approach using a systematic grid search over possible time and spatial centroid positions in the regional distance range and subsequent moment tensor inversion on longperiod time domain waveforms is used by H. Kawakatsu (ERI Tokyo University) and is published on http://wwwweic.eri.u-tokyo.ac.jp/GRiD_MT/.

The following table summarizes specific aspects of the published catalogs.

Table 3 list of published moment tensor catalogs

| Service | Range | Data, bandwidth | Greens functions | Constraints | Additional parameter | Error bounds | Inversion type |
|-----------|---|--|---------------------------|-------------|----------------------------|---|------------------------|
| CMT | worldwide since 1976 M > 5 | long-period BW and SW, 40-150 s | normal mode summation | deviatoric | centroid location and time | provided for MT elements | manually revised |
| GFZ | worldwide since 2011 M > 4.5 | complete seismograms 4.5 < M < 5.5 BW and SW 30-80 s 5 < M < 6.5 BW 40-100 s, SW 60-150 s 6 < M < 7 BW 60-150, SW 80-200 s M > 6.5 BW and SW 90-300 s M > 7.5 BW and SW 200-600 s M > 8.5 BW and SW 200-1000 s | reflectivity method | deviatoric | centroid depth | | automatic plus revised |
| GFZ-KIWI | worldwide since 2012 M > 5.5 | BW and SW 20-100 s | Gemini & QSSP | deviatoric | centroid location and time | yes | automatic |
| USGS | worldwide | Longperiod BW | ray synthetics | deviatoric | centroid depth | variance reduction | automatic and revised |
| USGS CMT | worldwide | Complete longperiod waveforms | full waveform synthetics | deviatoric | centroid location and time | variance reduction | automatic and revised |
| USGS, ERI | worldwide since 1990 M > 6.5 | W-phase 5.5 < M < 6.5 50-150 s 6.5 < M < 7 100-500 s 7 < M < 7.5 100-600 s 7.5 < M < 8 200-600 s M >= 8.0 200-1000 s | full waveform synthetics | deviatoric | centroid location and time | variance reduction | automatic and revised |
| BSL | regional Northern California) since 1993 M > 3.5 | complete long-period waveforms M > 3.5, 10-50 s 3.5 < M < 5 20-50 s M > 5 20-100 s | full waveform synthetics | deviatoric | centroid location and time | variance reduction, comparison of data and synthetics | Automatic and revised |
| SCEC | regional (southern California) since 2000 M > 3.5 | complete long-period waveforms | full wave form synthetics | deviatoric | Centroid location and time | variance reduction, comparison of data and synthetics | automatic and revised |
| INGV | regional (Mediterranean) M > 3.5 | SW spectra and waveforms | full waveform synthetics | deviatoric | centroid location and time | comparison of data and synthetics | automatic and revised |

| | | | | | | | |
|-----|---|--|--------------------------------|------------|----------------------------------|--|-----------|
| SED | regional (Switzerland and vicinity) since 1999 $M > 3.0$ | complete long-period waveforms | full waveform synthetics | deviatoric | centroid depth | comp. of data and synthetics | automatic |
| IGN | regional (Spain and surroundings) since 2002 $M > 3.5$ | complete long-period waveforms $M > 3.5$ 10-50 s $3.5 < M < 5$ 20-50 s $M > 5$ 20-100 s | full waveform synthetics | deviatoric | | variance reduction, compari- son of data and synthetics | automatic |
| ERI | regional (Japan) since 2003 $M > 3.5$ | long-period complete waveforms LP at 10 s | full waveform synthetics | deviatoric | centroid location and time | variance reduction | automatic |

7 Acknowledgments

Many students, course participants and colleagues helped improving the material over the years. We thank Peter Bormann for his persistent requests and reminders to deliver and improve the information sheets. We acknowledge the suggestions for improvement and careful reviews of Jochen Braunmiller, Daniela Kühn, Peter Bormann and Stefanie Donner.

8 References

- Aki, K., and Richards, P. G. (2002). Quantitative seismology. Second Edition, ISBN 0-935702-96-2, *University Science Books*, Sausalito, CA., 700 pp.
- Aster, R. C., Borchers, B., and Thurber, C. H., (2013). *Parameter estimation and inverse problems*, 2nd edition, Elsevier, ISBN: 978-0-12-385048-5.
- Bhattacharya, S., 1996. Earth-flattening transformation for P-SV waves (short note). *Bull. Seism. Soc. Am.*, **86**, 1979–1982.
- Ben-Menahem, A., and Singh, S.J. (2000). *Seismic Waves and Sources*. 2nd edition, Dover Publications, New York.
- Bernardi, F., Braunmiller, J., Kradolfer U., and Giardini, D. (2004). Automatic regional moment tensor inversion in the European-Mediterranean region. *Geophys. J. Int.*, **157** (2): 703-716; doi: 10.1111/j.1365-246X.2004.02215.x.
- Bukchin, E., Clevede, E., and Mostinskiy, A. (2010) Uncertainty of moment tensor determination from surface wave analysis for shallow earthquakes. *J. Seismol.*; doi: 10.1007/s10950-009-9185-8.
- Braunmiller J., Kradolfer U., Baer M., and Giardini D. (2002). Regional moment tensor determination in the European-Mediterranean region-initial results. *Tectonophysics*, **356**, 5–22.
- Cesca, S., Buorn, E., and Dahm, T, (2006). Amplitude spectra moment tensor inversion of shallow earthquakes in Spain. *Geophys. J. Int.*; doi:10.1111/j.1365-246X.2006.03073.
- Cesca, S., and Dahm, T. (2007). A frequency domain inversion code to retrieve time-dependent parameters of very long period volcanic sources. *Computer and Geosciences*; doi: 10.1017/j.cageo.2007.03.018.

- Cesca, S., Heimann, S., Stammmer, K., and Dahm, T. (2010). Automated procedure for point and kinematic source inversion at regional distances. *J. Geophys. Res.*, doi:10.1029/2009JB006450
- Cesca, S. and Heimann, S., and Dahm, T. (2010b). Rapid directivity detection by azimuthal spectra inversion. *J. Seismol.*, 15(1), 147-164; doi: 10.1007/s10950-010-9217-.
- Chapman, C. (1973). The earth flattening transformation in body wave theory. *Geophys. J. R. Astron. Soc.*, **35**, 55–70.
- Clinton, J. F., Hauksson, E., and Solanki, K. (2006). An evaluation of the SCSN moment tensor solutions: Robustness of the M_w magnitude scale, style of faulting and automation of the method. *Bull. Seism. Soc. Am.*, **96** (5), 1689-1705.
- Dahlen, F. A., and Tromp, J. (1998). *Theoretical Global Seismology*. Princeton University Press, pp. 944..
- Dahm, T. (1993). Relative moment tensor inversion to determine the radiation pattern of seismic sources (in German). PhD thesis, Institute for Geophysics, University of Karlsruhe, Germany, 121 pp.
- Dahm, T. (1996). Relative moment tensor inversion based on ray theory: theory and synthetic tests. *Geophys. J. Int.*, **124**, 245-257.
- Dahm, T., and Brandsdottir, B. (1997). Moment tensors of micro-earthquakes from the Eyjafjallajokull volcano in South Iceland *Geophys. J. Int.*, **130**, 183-192.
- Dahm, T., and Manthei, G. and Eisenblätter, J. (1999). Automated moment tensor inversion to estimate source mechanisms of hydraulically induced micro-seismicity in salt rock. *Tectonophysics.*, **306**, 1-17.
- Dahm, T., Krüger, F., Stammmer, K., Klinge, K., Kind, R., Wylegalla, K., Grasso, J.-R.(2007). The 2004 M_w 4.4 Rotenburg, Northern Germany, earthquake and its possible relationship with gas recovery. *Bull. Seism. Soc. Am.*, **97**(3), 691-704.
- Das, S., and Kostrov, B. V. (1988). *Principles of earthquake source mechanics*. Cambridge University Press.
- Donner, S., Rößler, D., Krüger, F., Ghods, A. and Strecker, M. (2013). Segmented seismicity of the M_w 6.2 Baladeh earthquake sequence (Alborz mountains, Iran) revealed from regional moment. *J. Seismol.*, **17**, 925-959; doi: 10.1007/s10950-013-9362-7.
- Doornbos, D. J. (Ed.) (1988). Seismological algorithms, computational methods and computer programs. *Academic Press*, New York, xvii + 469 pp.
- Dreger, D. S., and Helmberger, D. V. (1993). Determination of source parameters at regional distances with three-component sparse network data, *J. Geophys. Res.*, **98**, no. B5, 8107–8126.
- Dreger, D. S. (2003). 85.11 TDMT_INV: Time Domain Seismic Moment Tensor INVersion, In: Lee, W. H. K., Kanamori, H., Jennings, P. C., and Kisslinger, C. (Eds.). *International Handbook of Earthquake and Engineering Seismology*, Academic Press, Amsterdam, Part B, p 1627.
- Dufumier, H., and Cara, M. (1995). On the limits of linear moment tensor inversion of surface wave spectra. *Pageoph*, **145**, 235-257.
- Dufumier, H. (1996). On the limits of linear moment tensor inversion of teleseismic body wave spectra. *Pageoph*, **147**, 467-482.
- Duputel, Z., Rivera, L., Kanamori, H., and Hayes, G. (2012). W-phase fast source inversion for moderate to large earthquakes (1990-2010), *Geophys. J. Int.*, **189**(2), 1125-1147.

- Dziewonski, A. M., Chou, T.-A., and Woodhouse, J. H. (1981). Determination of earthquake source parameters from waveform data for studies of global and regional seismicity. *J. Geophys. Res.*, **86**, 2825-2852.
- Ebel, J. E., and Bonjer, K. P. (1990). Moment tensor inversion of small earthquakes in southwestern Germany for the fault plane solution. *Geophys. J. Int.* 101(1), 133-146.
- Ekström, G., Nettles, M., and Dziewonski, A. M. (2012). The global CMT project 2004-2010: Centroid-moment tensors for 13,017 earthquakes. *Phys. Earth Planet Int.*, **200-201**, 1-9.
- Ford, S., Dreger, D., and Walter, W. (2008). Source characterization of the August 6, 2007 Crandell Canyon Mine seismic event. *Seismol. Res. Lett.*, **79**, 637-644.
- Friederich, W., and Dalkolmo, J. (1995): Complete synthetic seismograms for a spherically symmetric earth by a numerical computation of the Green's function in the frequency domain. *Geophys. J. Int.*, **122**, 537-550.
- Frohlich, C., (1995). Characteristics of well-determined non-double-couple earthquakes in the Harvard CMT catalog. *Phys. Earth Planet. Inter.*, **91**, 213-228.
- Heimann, S. (2011). A Robust Method to estimate kinematic earthquake source parameters, Universität Hamburg, PhD thesis.
- Heimann, S., González, A., Cesca, S., Wang, R., Dahm, T. (2013). Seismic characterization of the terminal explosion of the Chelyabinsk meteor. *Geophys. Res. Lett.*, **84**(6), 1021-1025; doi: 10.1785/0220130042.
- Hudson, J. A., Pearce, R. G., and Rogers, R. M. (1989). Source type plot for inversion of the moment tensor. *J. Geophys. Res.*, **94** B1, 765-774.
- Jost, M. L., and Hermann, R. B. (1989). A students guide to and review of moment tensors. *Seism. Res. Lett.*, **60**, 37-57.
- Kanamori, H. (1993). W Phase, *Geophys. Res. Lett.*, **20**, 1691-1694.
- Kanamori, H., and Rivera, L. (2008). Source inversion of the W phase: speeding tsunami warning. *Geophys. J. Int.*, **175**, 222-238.
- Kennett, B. L. N., (1988). Systematic approximations to the seismic wavefields, In: Doornbos (1988), 237-259.
- Kikuchi, M., and Kanamori, H. (1991). Inversion of complex body waves – III. *Bull. Seism. Soc. Am.*, **81**, 2335-2350.
- Kravanja, S., Panza, G. F., and Šilený, J. (1999). Robust retrieval of a seismic point-source function. *Geophys. J. Int.*, **136**, 385-394.
- Krieger, L. (2011). Automated inversion of long period signals from shallow volcanic and induced seismic events. Dissertation, Fakultät für Mathematik, Informatik und Naturwissenschaften, Universität Hamburg.
- Krieger, L. and Heimann, S. (2012). MoPaD – Moment tensor plotting and decomposition: A tool for graphical and numerical analysis of seismic moment tensors. *Seism. Res. Lett.*, **83**(3), 589-595, doi: 10.1785/gssrl.83.3.589.
- Kuge, K., and Kawakatsu, H. (1990). Analysis of a deep “non double couple” earthquake using very broadband data, *Geophys. Res. Lett.*, **17**, 227-230.
- Lay, T., and Wallace, T. C. (1995). *Modern global seismology*. ISBN 0-12-732870-X, Academic Press, 521 pp.
- Menke, W. (1989). *Geophysical data analysis: discrete inverse theory*. Revised edition, Academic Press Inc., Orlando, Florida, 260 pp..

- Müller, G. (1973). Seismic moment and long period radiation of underground nuclear explosions. *Bull. Seism. Soc. Am.*, **3**, 847-857.
- Müller, G. (1977). Earth-flattening approximation for body-waves derived from geometric ray theory – Improvements, corrections and range of applicability. *J. Geophys.*, **42**, 429– 436.
- Müller, G. (1985). The reflectivity method: A tutorial. *J. Geophys.*, **58**, 153-174.
- Müller, G. (2001). Volume change of seismic sources from moment tensors. *Bull. Seism. Soc. Am.*, **91**, 880-884.
- Nabelek, J. (1984). Determination of earthquake source parameters from inversion of body waves. Ph.D. thesis, Mass. Inst. of Tech.
- Oncescu, M. C. (1986). Relative seismic moment tensor determination for Vrancea intermediate depth earthquakes, *Pageoph*, **124**, 931-940.
- Pondrelli, S., Salimbeni, S., Ekström, G., Morelli, A., Gasperini, P., and Vannucci, G. (2006). The Italian CMT dataset from 1977 to the present, *Phys. Earth Planet. Int.* **159**(3-4), 286-303; doi:10.1016/j.pepi.2006.07.008
- Pondrelli S., Salimbeni S., Morelli A., Ekström G., Postpischl L., Vannucci G., and Boschi E. (2011). European-Mediterranean Regional Centroid Moment Tensor Catalog: solutions for 2005-2008. *Phys. Earth Planet. Int.*; doi: 10.1016/J.PEPI.2011.01.007.
- Press, W. H., Teukolsky, S. A., Vetterlin, W. T., and Flannery, B. P. (2007). *Numerical Recipes: The Art of Scientific Computing, Third Edition*, Cambridge University Press (ISBN-10: 0521880688, or ISBN-13: 978-0521880688).
- Riedesel, M., and Jordan, Th. H. (1998). Display and assessment of seismic moment tensors. *Bull. Seism. Soc. Am.*, **79**(1), 85-100.
- Shao, J., and Tu, D. (1995). The Jackknife and Bootstrap. *Springer Series in Statistics*.
- Šilený, J., Panza, G. F., and Campus, P. (1992). Waveform inversion for point source moment retrieval with variable hypocentral depth and structural model. *Geophys. J. Int.*, **109**, 259-274.
- Šilený, J., and Pšenčík, I. (1995). Mechanisms of local earthquakes in 3-D inhomogeneous media determined by waveform inversion. *Geophys. J. Int.*, **121**, 459-474.
- Šilený, J., Campus, P., and Panza, G. F. (1996). Seismic moment tensor resolution by waveform inversion of a few local noisy records - I. Synthetic tests. *Geophys. J. Int.*, **126**, 605-619.
- Sipkin, S. A. (1982). Estimation of earthquake source parameters by the inversion of waveform data: synthetic waveforms. *Phys. Earth Planet. Inter.*, **30**, 242-259.
- Sokos, E., and Zahradník, J., (2008). ISOLA: a Fortran code and a Matlab GUI to perform multiple-point source inversion of seismic data, *Computers and Geosciences*, **34**, 967-977.
- Sokos, E., and Zahradník, J. (2013). Evaluating centroid moment tensor uncertainty in new version of ISOLA software. *Seismol. Res. Letters*, **84**, 656-665.
- Stein, S., and Okal, E. (2005). Speed and size of the Sumatra earthquake. *Nature* **434**, 581-582
- Stein, S., and Wysession, M. (2003). *An introduction to seismology, earthquakes and Earth structure*. Blackwell Publishing, Oxford.
- Tanioka, Y., and Ruff, L. (1997). Source time functions. *Seism. Res. Lett.*, **68**, 386-400.

- Tocheport, A., Rivera, L., and Chevrot, S. (2007). A systematic study of source time functions and moment tensors of intermediate and deep earthquake. *J. Geophys. Res.*; doi: 10.1029/2006JB004534
- Tibi, R., Bock, G., Xia, Y., Baumbach, M., Grosser, H., Milkereit, C., Karakisa, S., Zünbül, S., Kind, R., and Zschau, J. (2001). Rupture processes of the 1999 August 17 Izmit, and November 12 Düzce (Turkey) earthquakes. *Geophys. J. Int.*, **144**, F1-F7.
- Tsai, V. C., Nettles, M., Ekström, G., and Dziewonski, A., 2005. Multiple CMT source analysis of the 2004 Sumatra earthquake. *Geophysical Research Letters*, **32**; L17304, doi: 10.1029/2005GL023813.
- Tape, W., and Tape, C. (2012). A geometric comparison of source-type plots. *Geophysical J. Int.*, **190**, 499-510; doi: 10.1111/j.1365-246X.2012.05490.x.
- Udías, A. (1999). *Principles of Seismology*. Cambridge University Press, United Kingdom, 475 pp.
- Valentine, A.P., and Trampert, J. (2012). Assessing the uncertainties on seismic source parameters: Towards realistic error estimates for centroid-moment-tensor determinations, *Phys..Earth Planet. Inter.*, **210**, 36-49.
- Vallée, M., Charléty, J., Ferreira, A. M. G., Delouis, B., and Vergoz, J. (2011). SCARDEC: a new technique for the rapid determination of seismic moment magnitude, focal mechanism and source time functions for large earthquakes using body wave deconvolution, *Geophys. J. Int.*, **184**, 338-358.
- Vasco, D.W., (1989). Deriving source-time functions using principle component analysis. *Bull. Seism. Soc. Am.*, **79**, 711-730.
- Vavryčuk, V. (2001). Inversion for parameters of tensile earthquakes. *J. Geophys. Res.*, **106**(B8), 16339–16355; doi:10.1029/2001JB000372.
- Vavryčuk, V., and Kuehn, D. (2012). Moment tensor inversion of waveforms: a two-step time-frequency approach. *Geophys. J. Int.*, **190**, 1761-1776.
- Wang, R. (1997). Tidal response of the solid earth. In H. Wilhelm, W. Zürn and H. G. Wenzel (Eds.). *Tidal phenomena, Lecture Notes in Earth Sciences*, Vol. **66**, pp. 27-57, Springer-Verlag, Berlin/Heidelberg.
- Wang, R. (1999). A simple orthonormalization method for stable and efficient computation of Green's functions. *Bull.Seism. Soc. Am.*, **89**(3), 733-741.
- Wiggins, R. A., and Robinson, E. A. (1965). Recursive solution to the multichannel filtering problem. *J. Geophys. Res.*, **70**, 8, 2156-2202; doi: 10.1029/JZ070i008p01885.
- Whidden, K. M., Rudzinski, L., Lizurek, G., Pankow, K. L. (2013). Regional, local and in-mine moment tensors for the 2013 Rudna mine collapse, Poland. AGU 2013 fall meeting, 5210-2396
- Zahradník, J., and Custódio, S. (2012). Moment tensor resolvability: Application to Southwest Iberia. *Bull. Seism. Soc. Am.*, **102**, 1235-1254.
- Zhang, Y., Wang, R., Zschau, J., Chen, Y.-T., Parolai, S., Dahm, T. (2014). Automatic imaging of earthquake rupture processes by iterative deconvolution and stacking of high-rate GPS and strong motion. *J. Geophys. Res.*, doi: 10.1002/2013JB010469